Institute of Materials Research

51170 Köln

German Aerospace Center

DLR

REVIEW OF AERONAUTICAL FATIGUE INVESTIGATIONS IN GERMANY DURING THE PERIOD MAY 2001 TO MARCH 2003

compiled by Claudio Dalle Donne

April 2003

1 INTRODUCTION

The review has been prepared for presentation at 2003 Meeting of the International Committee on Aeronautical Fatigue in Lucerne Switzerland, 5.-6. May 2003. German aerospace manufacturers, governmental and private research institutes, aerospace authorities as well as universities were invited to contribute summaries of aeronautical fatigue related research activities. These voluntary contributions are compiled here. The author acknowledges these contributions with appreciation. Enquiries should be addressed to the authors of the summaries.

Mailing Addresses of Contributing Companies and Institutes:

Airbus-D	Airbus Deutschland GmbH, Kreetslag 10, 21129 Hamburg
EADS-M	European Aeronautic Defence and Space Company, Military Aircraft, 81663 Munich
DLR-BK	German Aerospace Center DLR, Institute of Structures and Design, PO box 80 03 20, 70503 Stuttgart
DLR-SM	German Aerospace Center DLR, Institute of Structural Mechanics, Lilienthalplatz 7, 38108 Braunschweig
DLR-WF	German Aerospace Center DLR, Institute of Materials Research, 51170 Cologne
Grob	Grob Aerospace, Lettenbachstr. 9, 86874 Tussenhausen-Mattsies
IABG	Industrieanlagen-Betriebsgesellschaft mbH, PO-Box 1212, 85503 Ottobrunn
IMA	Materialforschung und Anwendungstechnik GmbH, PO-Box 800144, 01101 Dresden
LBF	Fraunhofer Institute for Structural Durability LBF, Bartningstr. 47, 64289 Darmstadt
Liebherr	Liebherr Aerospace GmbH, 88161 Lindenberg
MAN	MAN Technologie AG, Franz-Josef-Strauß-Straße 5, 86153 Augsburg
MPA	Staatliche Materialprüfungsanstalt (MPA), Universität Stuttgart, Pfaffenwaldring 32, 70569 Stuttgart
TU-HH	TU Hamburg-Harburg, Polymers & Composites, Denickestrasse 15, 21073 Hamburg
UniBw-M	University of the Federal Armed Forces Munich, Department of Materials Science, 85577 Neubiberg
USI	University of Siegen, Department of Materials Science and Testing, 57068 Siegen

2 FULL SCALE TESTING

2.1 Overview of Full Scale Fatigue Tests in Germany (March 2003)

A/C Project	Customer	Test Structure	Time Schedule	Test Lab	Chapter
TANGO	Airbus-D	metallic and composite barrel, curved fuselage panels	2002-2004	Airbus-D, IMA	2001 Review, 3.1
A340-600	Airbus-D	center fuselage and wing	2001-2003	IMA, IABG	2001 Review
A340-500/600	Airbus-D	rear fuselage	2001-2002	Airbus-D	2001 Review
AIR	Airbus-D	aluminum integral fuselage barrel	1999-2003	Airbus-D, IMA	4.1
A380	Airbus-D	megaliner barrel	2002-2004	Airbus-D	2.6
Eurofighter	EADS-M	wing attachment box	2001-	EADS-M	2.3
Eurofighter	EADS-M	main landing gear, nose landing gear	2000-2001	IABG	2.4
MAKO	EADS-M	taileron	2003	EADS-M	2.5
Vigilant G 109B	Grob	fuselage and wings	2003	Grob	2.2
ERJ-170	Liebherr	main landing gear fitting	2002	IMA	2.8
PC12	Pilatus Aircraft Ltd.	pessure dome	2001	IABG	Swiss Review
F/A-18	RUAG (CH)	complete airframe	1998-2002	IABG, RUAG	Swiss Review

2.2 Full Scale Fatigue Test of the Grob Vigilant G 109B

Paul Antemia (Grob)

The Grob Vigilant G 109B is a low-wing, all composite motorglider with a wing span of 17.4 m and a fuselage length of 8.1 m. A complete Vigilant (G 109B) aircraft structure was manufactured for the fatigue test during the Vigilant/Air Cadets serial production for the RAF. The composite structure was equipped with engine frame and undercarriage. The investigation area is the wing root, wing stubs and fittings in fuselage. For reduction of the test area, the wings were cut at 4300 mm span position allowing the application of the maximum (shear and bending) load on the wing root area, with a simpler rig, Fig. 1. The wing extremities have been locally reinforced to support the higher reaction forces corresponding to the root section.

The fatigue test was performed using the operational load measurements (OLM) established by QinetiQ. The measured strains on the left wing and on the undercarriage during the test flights were analysed and the corresponding load levels were established. The OLM were performed on four airfields with different run and taxiway surfaces.

A total of 61180 FH were simulated. During the first 25500 FH the loads were applied by an hydraulic installation, whereas during the remaining 35680 FH the loads were introduced to the main structure by electric actuators.

After the fatigue test a residual strength test was carried out on the wing fuselage structure. The test was executed at a temperature of at least 54° C to meet the most unfavourable environmental condition.

The fatigue test and the residual strength test demonstrated that after applying fatigue loads corresponding to 61180 FH, the structure was able to carry the limit load without permanent deformation and an ultimate load corresponding to a safety factor of j = 1.1 (x limit load).

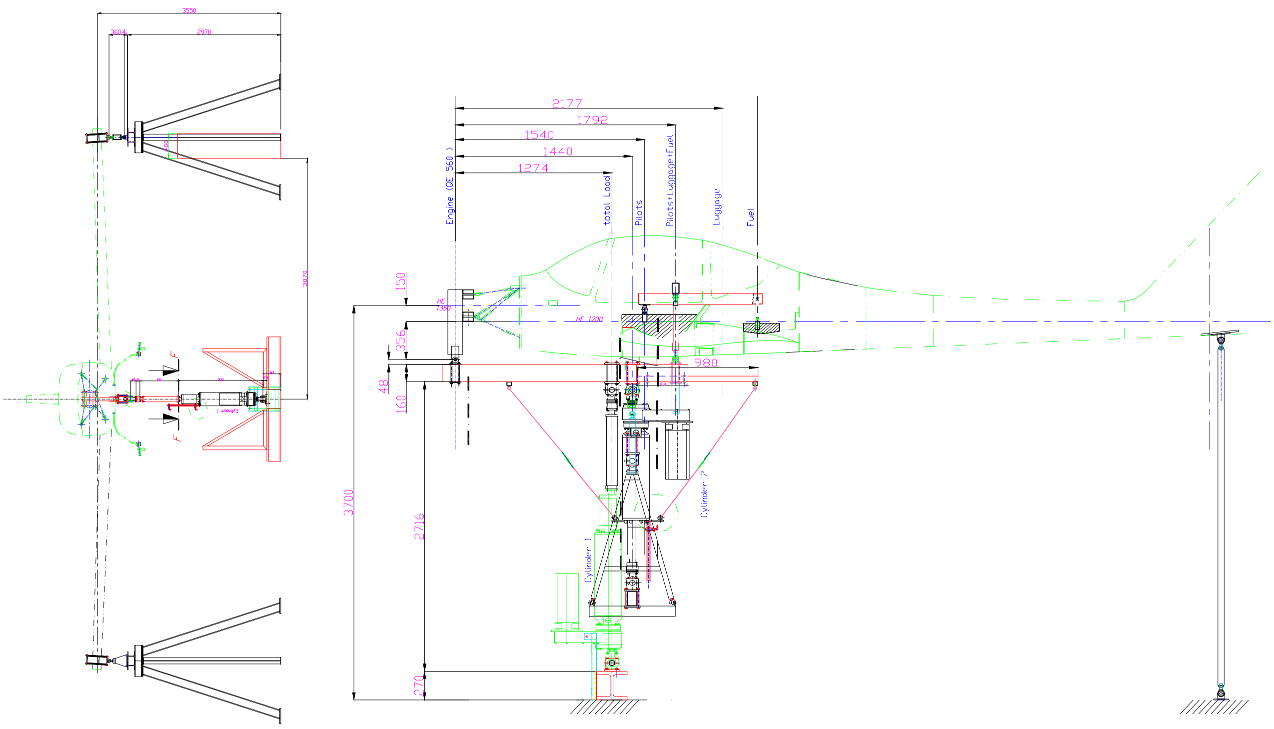

Fig. 1: Front and side view of the Grob Vigilant G 109B test set-up.

Taking into account the requirements of JAR 23.573 (a3), these results may lead to the conclusion that applying a reduction factor 5 for the simulated period 61180 FH, a life of 12236 FH has been demonstrated by testing the structure under operational conditions. The new design of the landing gear leg is able to support more than 50000 landings estimated for the whole operational life of the aircraft. This affirmation is demonstrated by fatigue analysis of QinetiQ and by static tests performed on the landing gear leg [1].

2.3 Wing Attachment Box Fatigue Tests

A. McCarthy (EADS-M)

The Wing Attachment Box (WAB) fatigue test program forms a major contribution to the qualification route for the Eurofighter centre fuselage wing attachment structure with special emphasis on the major frames, carbon fibre composite (CFC) skin and fuel tanks.

An additional goal of the test is to qualify the damage tolerance of the laser welding manufacturing technique for the intake duct Al-Li panels. The LH intake duct is manufactured using the Nd-YAG laser welding process for incorporation of stiffening ribs whereas the RH duct skin incorporates integrally machined ribs. Hence a comparison of the performance of both techniques can be made.

The test is presently being performed at the EADS Structural Test Laboratory in Ottobrunn, Germany.

The WAB incorporates the aft centre fuselage which includes the three major attachment frames and the CFC outer skin. Wing loads are introduced into the frames by left- and right- hand wing dummies. To adequately simulate fuselage bending, a portion of the rear fuselage is included and loaded by an actuator and gantry simulating rear fuselage and engine vertical inertia effects. The structure is further extended forwards to a built-in frame where all forces are reacted into the test rig. Additional longitudinal loading is applied to the forward two main frames to simulate the restraint across the landing gear bay normally provided by the wing. Furthermore rigid rods are installed longitudinally between the wing dummies for the same purpose.

A randomised flight-by-flight test program of 18000 Simulated Flight Hours (SFH) is being simulated to verify the required 6000 operational flight hours (scatter factor of 3).

Manoeuvre load cases with fuel tank pressures (using water) as well as ground operations are included.

Environmental conditions are taken into account in so far that the fuel tank water is systematically heated to 95°C during the program to simulate the fuel temperature effects on the CFC skin.

Verification of the structural Finite Element Model (FEM) is an essential requirement of the test measurements and to this end a total of 730 strain gauge channels and 40 deflection transducers are attached and will produce the data for the evaluation of the structure. Static and dynamic measurements up to maximum loads in the fatigue spectrum have been carried out and will be repeated during the programme.

Static tests with local fuselage centre pylon store loads have also been performed.

Impacts of various intensities were applied to CFC components at high stressed areas of the longerons, frame flanges, ply drop off areas and one access cover. Using ultrasonic equipment these areas are being monitored throughout the test to substantiate the damage tolerance requirements.

Structural inspections are being conducted at selected intervals during the fatigue testing phase in accordance with the inspection procedures.

Applied actuator loads are monitored by load cells and compared with supply values.

Fuel tank pressures are monitored by pressure transducers and achieved temperatures by thermocouples.

The control system embodies closed loop digital servo controllers addressed by a host computer to command each loading channel simultaneously.

Following completion of fatigue testing up to 18000 SFH, certain static load cases will be taken to 80% ultimate design load at elevated temperature to demonstrate the required residual strength.

Finally, selected load cases will be taken to 100% design ultimate load at room temperature and one case taken to failure..

Up to date 8000 Flight Hours have been simulated without problems.

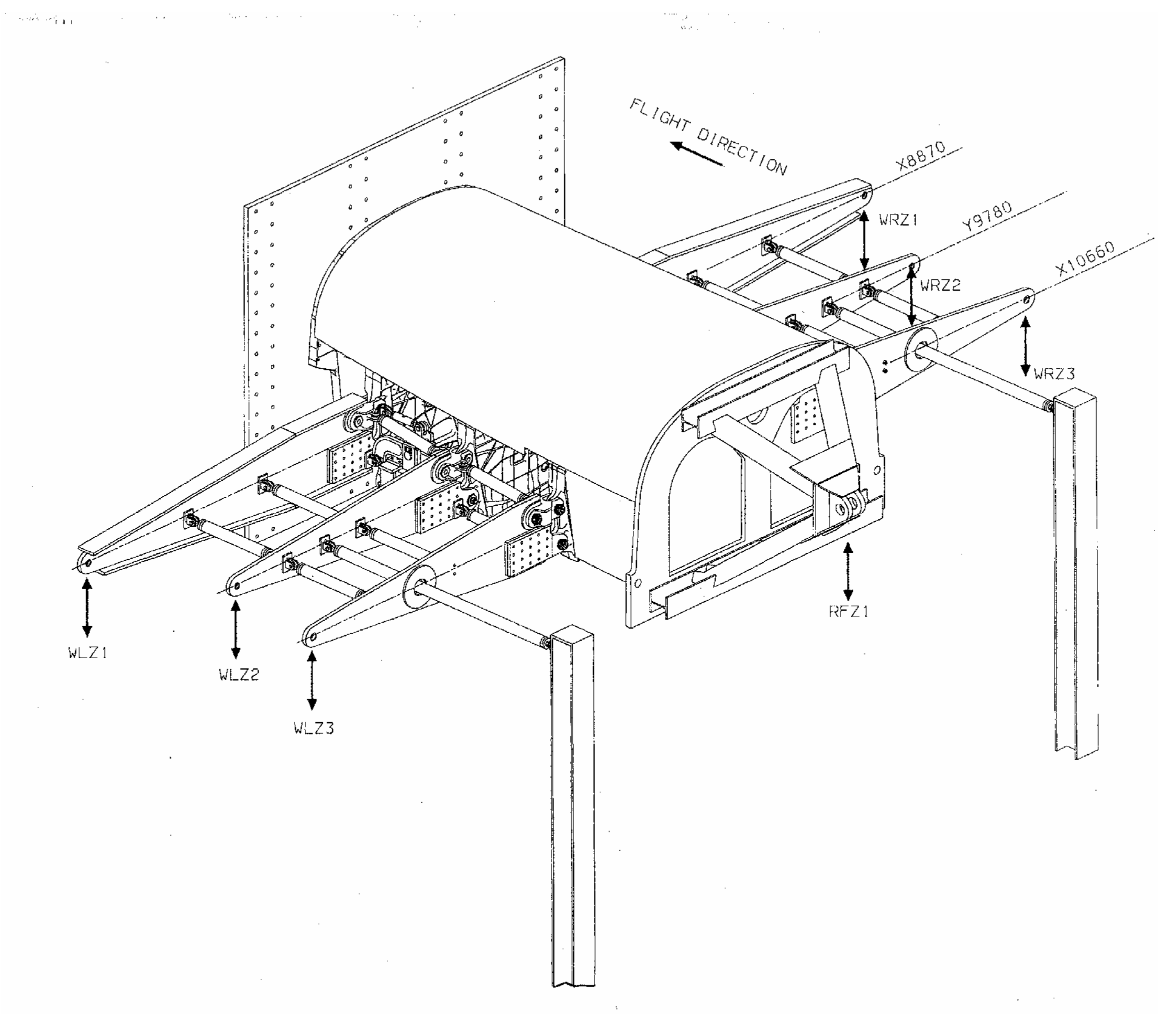

Fig. 2: Schematic of Eurofighter wing attachment box fatigue test set up.

2.4 EF2000: Nose Landing Gear Full Scale Fatigue Test

M. Wandel, U. Soetebier (Liebherr) and R. Dilger (EADS-M)

The contractual qualification of the nose landing gear (NLG) structure against the fatigue requirements (6000 FH, 8000 Landings, 10000 Retraction/Lowering Cycles, Scatter Factor = 3) of the Eurofighter EF2000 undercarriage specification is based on the results of a full scale fatigue test together with calculated read across. The nose landing gear was designed and is tested under the responsibility of Liebherr Aerospace GmbH in Lindenberg/Germany.

The full scale fatigue test sample comprises a complete nose undercarriage structure and is subjected to an appropriate flight-by-flight loading spectrum. The loading spectrum is based on different take-off and landing masses and includes ground manoeuvres like turning, steering, braking, towing etc., retraction/lowering cycles as well as landing impacts for various sink rates and landing types (flared, non-flared). The shock absorber travel and the rolling radius of the tyre are fixed, based on a damage equivalent re-calculation of the applied loads.

Within the full scale fatigue test all structural significant NLG components are regularly subjected to a detailed NDT inspection. In December 2002, 15000 test hours (5000 qualified FH) were successfully achieved.

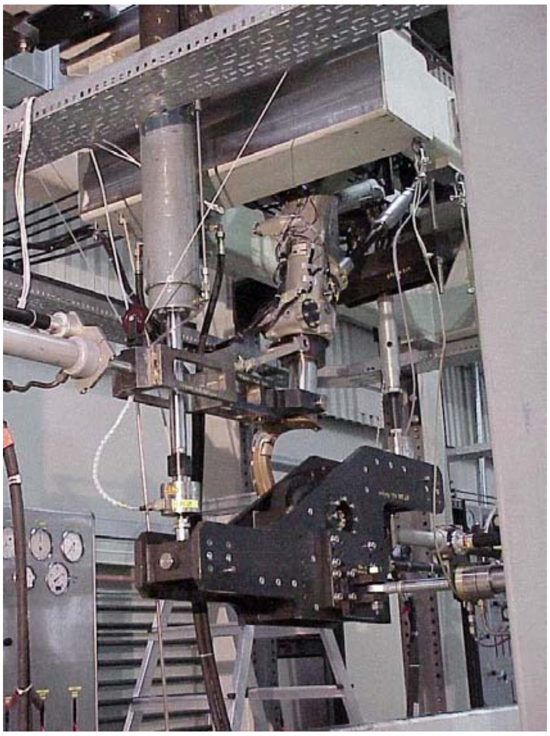

Fig. 3: Eurofighter nose landing gear test set-up.

2.5 MAKO Spigot Fatigue and Damage Tolerance Test

E. Stuible (EADS-M)

The taileron of the MAKO light combat and trainer aircraft was developed under the assumption of 10 000 FH design life and the damage tolerance concept. After 2 lives of the design fatigue spectra, initial cracks have to be applied into the structure at significant areas. After 2 further lives of the design fatigue spectra, 115% limit load will be statically applied and no failure of the structure is permitted to meet the damage tolerance requirements.

As a technology demonstrator, the taileron spigot has been selected to assess the damage tolerance design of a casted titanium part with the casting factor of 1,0. The MAKO taileron is composed of the titanium spigot, aluminium spars, ribs and CFC upper and lower skins. The loads are introduced by means of 3 hydraulic actuators and load trees into the taileron structure, see Fig. 4. The specimen is restrained against P_x, P_y, P_z and M_x, M_z at the inboard and outboard spigot bearings. Restraint against M_y (torsion) is provided by the original taileron actuator lever and a rigid actuator dummy at a representative angle.

A total of 167 Strain gauge channels are instrumented. The measured strains are periodically recorded for 3 specific limit load cases in order to validate the FEM Model and to find out changes in the load path as an indicator for the growth of the initial cracks.

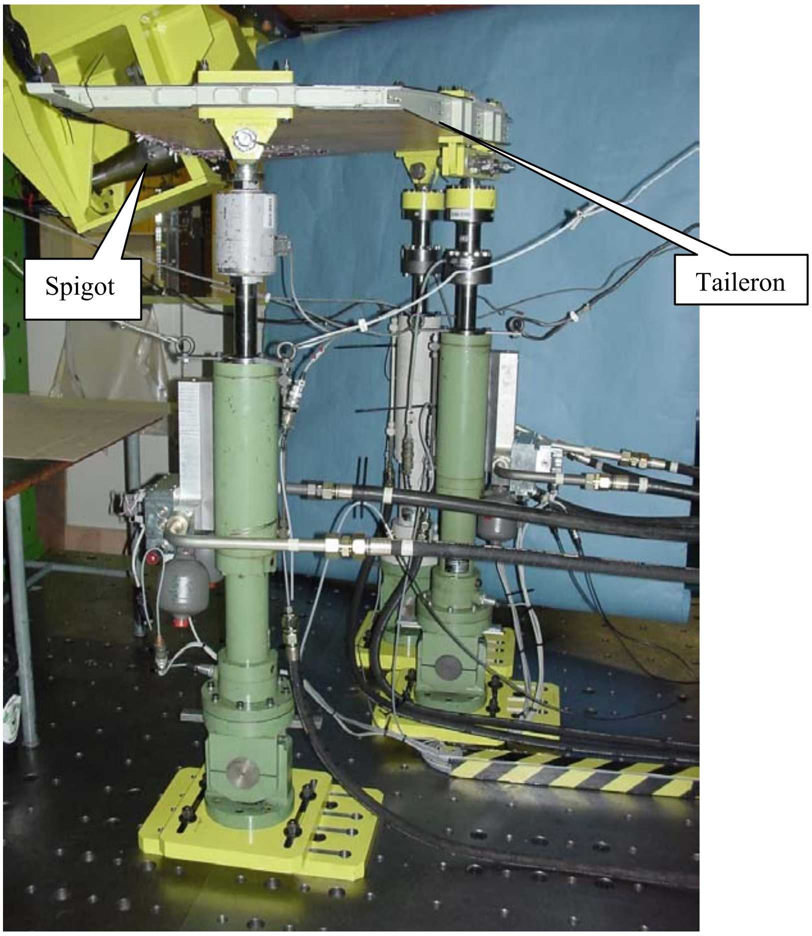

Fig. 4: MAKO taileron spigot test set-up.

Inspections of the titanium spigot, taileron lever, aluminium spars and the CFC skins will be performed at 0.5, 1, 2 design lives during the durability test phase and at 0.5, 1, 2 design lives during the damage tolerance test phase.

The test status at 01.03.2003:

- 6000 SFH corresponding to 6/40 design life without any damage.

2.6 Full Scale Fatigue Test of a Megaliner Type Fuselage Section

Achim Etzkorn (Airbus-D)

Designing a new aircraft in the size of a megaliner (aircraft for more than 550 people with two passenger and one cargo deck) is a challenge in means of the development of a pressurized fuselage. Due to the needed height and the limited width an oval cross section is recommended. Because of the new fuselage shape and weight requirements on such a big aircraft, progressive structural solutions with new materials or manufacturing techniques have to be developed. To minimize the risk of new materials or techniques, the structure has to be tested in full scale.

The megaliner barrel is a rear fuselage section of a megaliner type aircraft (see Fig. 5). Its total length is approx. 15 m, the width is 7,15 m and the height 8,69 m. The ends are closed by a fixed and a free pressure bulkhead. The inner structure of the barrel is represented by cross beams and seat tracks in main and upper deck and just cross beams in the cargo deck. The roof above upper deck and the cargo deck floor are stabilised by frameworks. To examine the behaviour of large cut outs in high loaded areas, two passenger doors are installed in the upper deck. The mounted doors are each produced by casting as one single part. Cut outs with cases for the emergency slides are located below those two doors. Furthermore there are 10 window cut outs at each side of the upper deck and 14 window cut outs on each side of the main deck. Some of the cut outs are closed by aluminium doublers, at other locations windows and window frames are mounted. Within the barrel new materials are introduced as well as new production and assembling techniques. In the upper fuselage section where high tensile loads occur, GLARE® represents a great amount of the skin. Because of the fibre orientation within this material it can withstand high tensile stresses. The stringers in the GLARE® area are made from monolithic aluminium as well as from GLARE®. The mounting technique of the stringers is riveting or bonding. In the region where shear is the main loading, monolithic aluminium alloys 2024A and 2524 are mainly used.

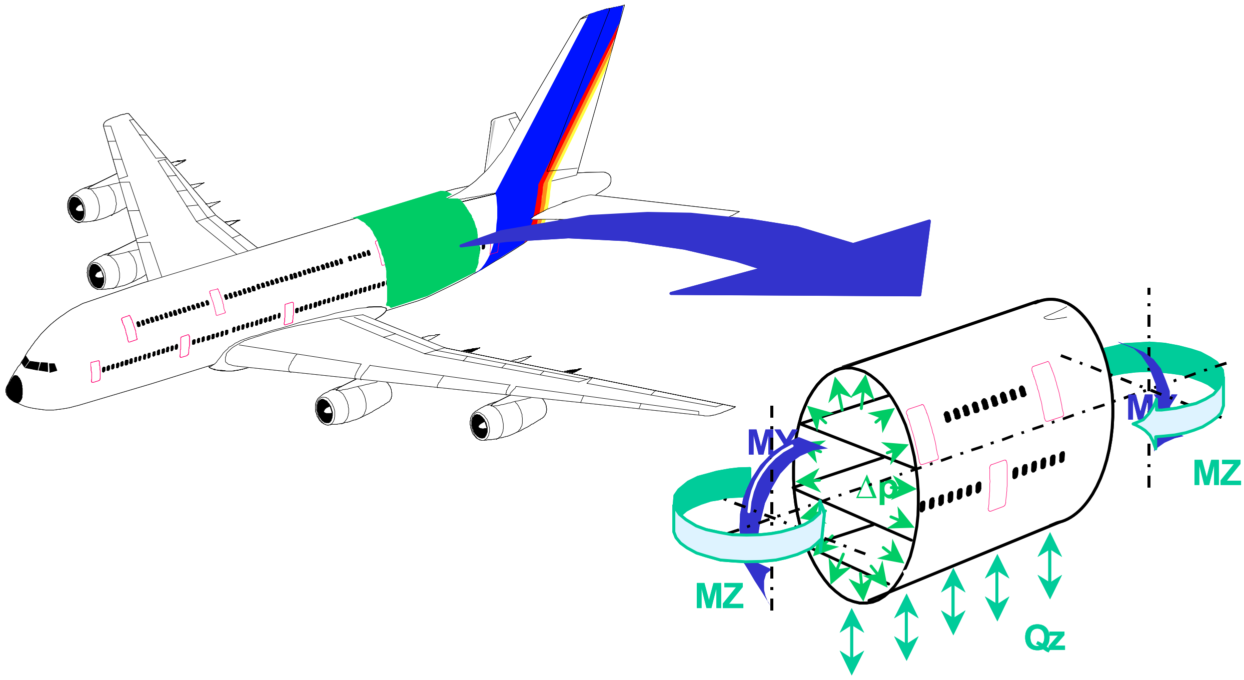

Fig. 5: Location of the barrel in a megaliner type aircraft.

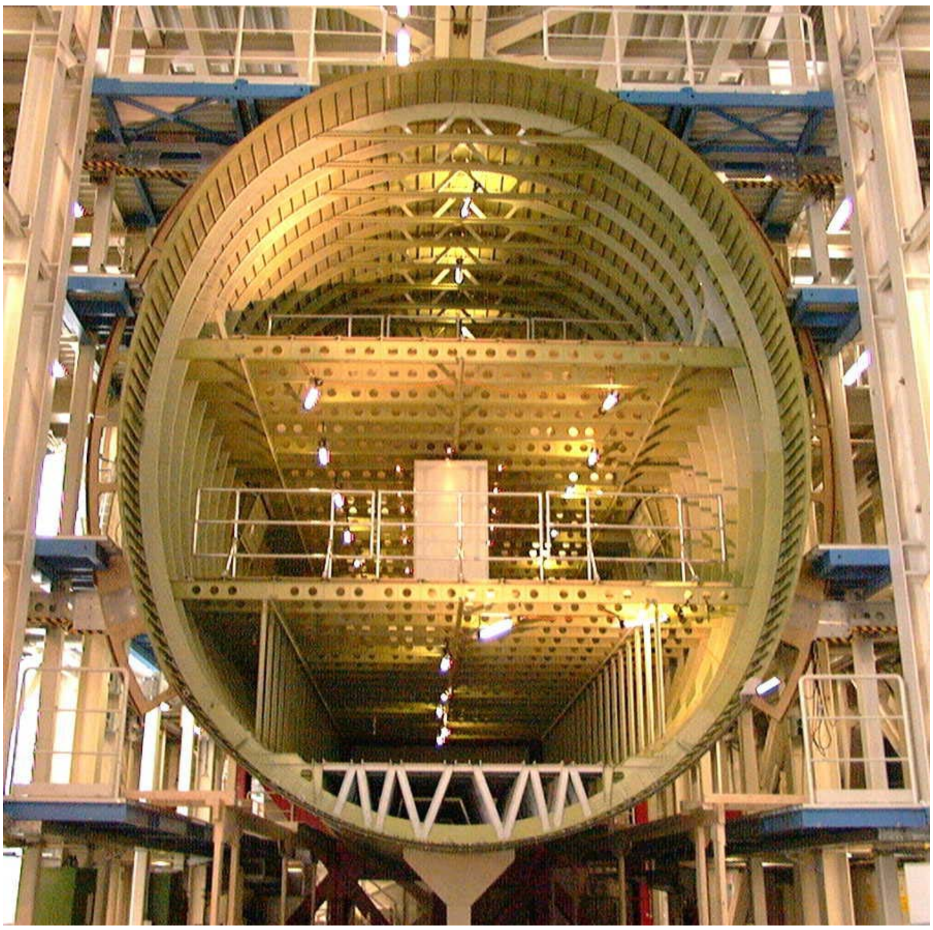

Fig. 6: Megaliner Barrel right after assembling.

The compressive loaded lower shell is produced out of 6013 or 6056, which are weldable alloys. In this region a great number of joints, clip/skin- and stringer/skin-connections, are produced by laser beam welding. Fig. 6 shows the megaliner barrel right after the assembly of the specimen and just before mounting the free pressure bulkhead with the loading systems.
The above described fuselage section is supposed to go through a full scale fatigue test and some static tests. The scheduled number of simulated flight cycles is 60.000 to reach twice the extended design service goal. The loads are introduced by hydraulic jacks. The load introductions for the bending moments M_Y and M_Z are mounted at the free bulkhead. Because of the oval cross section, torsion can not be put in at the free bulkhead. Therefore two load introduction devices are installed in tangential direction, one at the lower side close to the fixed bulkhead and one on the upper side close to the free bulkhead. To simulate the loading of the fuselage section with passengers and freight (Q_Z), all three decks of the barrel are loaded with wide branched load introduction devices. Finally the before mentioned load state is superimposed by Δp. The pressurization time is approx. 30 seconds. The intensity of any loading state is defined by a loading program which describes 8 different flight types of varying severity. The complete test is divided in 28 blocks with 2150 flights each. The distribution of the flight types within the blocks is randomised.

Up to now nearly 35.000 simulated flight cycles have been performed. During the cycling period the test is stopped every day for a visual inspection. Every 5.000 flights a major inspection including NDT testing is carried out. Locations which are defined as critical like special rivet holes or repair doublers are frequently dismounted and tested for example by roto-test. For an on-line investigation of the specimens behaviour approx. 2000 strain gages are bonded at locations of increased interest like for example door- and window surroundings.

Before the second life cycle (30.001-60.000) was started, artificial damages like cracks above broken stringers or frames and crack initiations at critical locations were introduced in areas made of both GLARE® and monolithic aluminium. The examination of the growing behaviour of those damages will be part of the upcoming phase.

2.7 A380-800 EF Full Scale Fatigue Test

S. Berssin (Airbus-D)

This review provides the actual status of the Full Scale Fatigue Test program EF, which will be performed in order to support the certification of the A380-800 Commercial Transport Aircraft according to the regulations FAR/JAR 25.571.

The A380EF will be performed by the IABG (Industrieanlagenbetriebsgesellschaft mbH) test laboratory in conjunction with the IMA test institute in Dresden.

The test is going to be started in November 2005. The main characteristics of the test are:

- Full aircraft testing (complete fuselage + wings, with shortened VTP and without HTP)
- Nearly 200 active hydraulic jacks to simulate air- and inertia loads
- Complex flight-by-flight loading program with an average of 480 loadcases per flight
- Three different missions applied
- Test goal 47500 FC (equivalent to 2.5 time designe service goal DSG)
- Load increase of 10% to cover weight variants and future developments
- Envisaged test speed of 900 FC / week
- Verification of fatigue and damage tolerance behavior for metallic and hybrid structures

Starting in 2000 and completed in March 2003, a new loading concept has been developed, which differs significantly from the previous AIRBUS Fatigue tests. The new loading concept reflects the special needs of a complete airframe testing, which is demanding for the specimen balance and reaction.

In parallel to the test loading concept development Airbus engineering departments worked on the loading program which in general contains:

- Simulated test loads (hydraulic jack loads) with 10 percent loads enhancement
- Ground steady loads (1g) with superimposed incremental loads for taxiing, turning, take-off, rotation, landing impact, landing run and braking,
- Flight steady loads (1g) with superimposed vertical and lateral incremental gust and manouvre loads,
- Corresponding cabin pressure differential for each flight phase based on the typical flight profile.

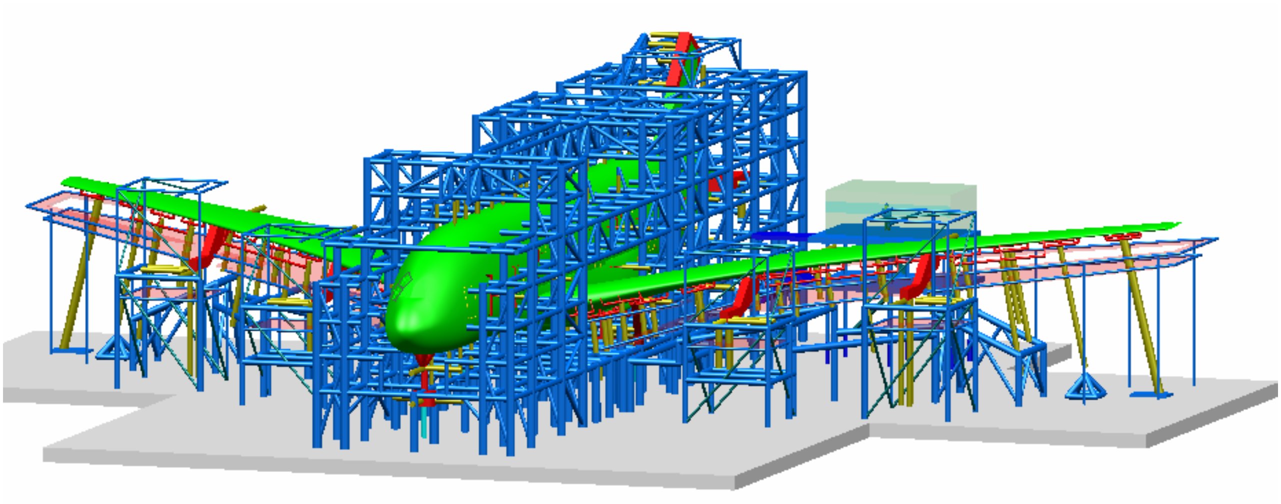

Fig. 7: A380EF test set-up overview.

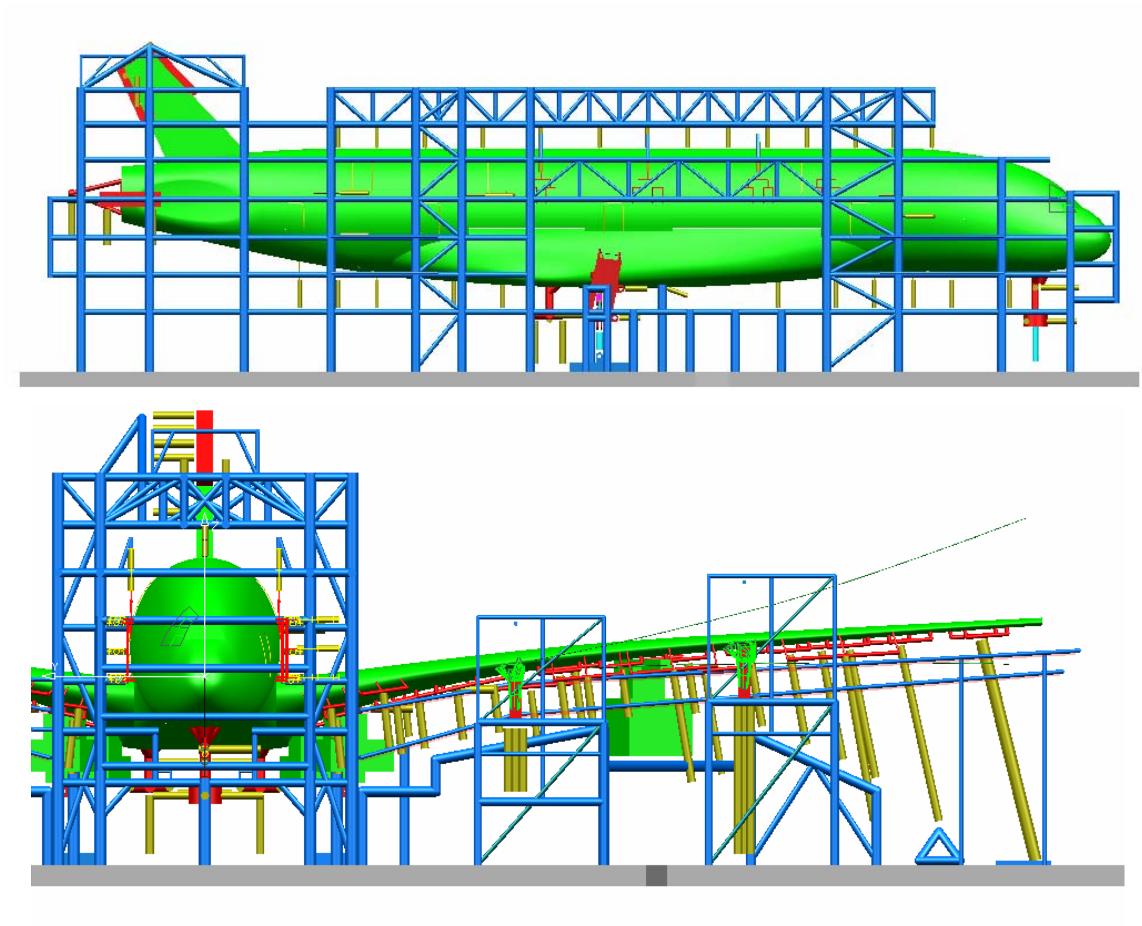

Fig. 8: A380EF Test set-up side and front views.

- Repeated blocks of individual flight types and different severity,
- 1900 flights per block representing a randomized distribution,
- 21 flight types including 8 different airborne sub-flight types and 3 different ground sub-flight types are foreseen,
- Random application of flight types and load cases.

This work will be continued until the fatigue test start, following the different loads loops of the aircraft.

The next step in the EF test set-up development will be the adaptation of the specimen design, which comprises the design of fuselage cut-outs for the hydraulic jacks and local reinforcement in areas of load introduction. The first aircraft part will than be delivered in September 2004.

The transportation of the specimen sections will be performed by barges on the river Elbe. In total, three different transports are necessary to bring all fuselage sections and the two wings to Dresden. The fuselage sections will than be joined-up in Dresden, followed by the wing/fuselage junction assembly. All Final Assembly work will be performed by AIRBUS personnel using standard Final Assembly procedures and means, in order to secure a full reproducibility of the structure.

The Final Assembly of the structure will be followed by a phase for completion of the test set-up and a commissioning phase.

The Full Scale Fatigue Test A380EF will than be started in November 2005, with the objective to reach 5000 simulated flights, which is equivalent to more than 5 years of safe operation, at time of Type Certification (January 2006).

2.8 Development Fatigue Test for the ERJ-170 Main Landing Gear Fitting

Peter Frömmel and Wolfgang Fessenmayer (IMA)

The German company Liebherr Aerospace GmbH develops and manufactures the main landing gear (MLG) for the new regional aircraft EMB-170 of EMBRAER. On behalf of Liebherr IMA GmbH Dresden carried out fatigue tests of the MLG main fitting retraction/lowering to reduce the development risk.

The test was divided in two parts:

- A static stress verification to verify the stress values determined by finite element analysis. For this reason linear strain gauges and rosettes were applied to the structure, which was subjected to several different load cases. The comparison of measured and calculated stress values was done by Liebherr.
- A fatigue test to prove, that the structure resists the retraction/lowering fatigue load spectrum without failures.

Together with Liebherr IMA Dresden worked out a modified test procedure with a simplified fatigue load sequence for

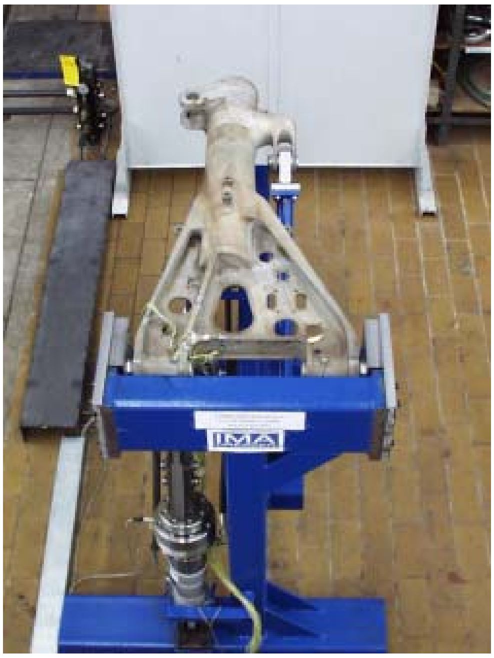

Fig. 9: Test set-up for the ERJ-170 main landing gear fitting.

the MLG main fitting. In this way the highly complex retraction/lowering loading situation could be simulated practically by means of a relative simple actuator configuration.

Fig. 9 shows the corresponding test rig with mounted test specimen and two acting actuators for the gear up and gear down forces.

The main fitting passed the test without any objections.

2.9 ARIANE 5 Booster: Full Scale Component Tests Carried out within the Qualification Programme

K. Reiling and H. Karl (MAN), E. Roos and W. Stadtmüller (MPA)

The European Ariane 4 rocket was launched for the last time in January 2003. This series will be replaced by a new one, Ariane 5, Fig. 10, designed for higher payload masses. Therefore, a new solid propulsion booster was developed to cope with the new and higher requirements. Part of the qualification programme were four full scale component tests using prototypes of the booster. The tests were carried out at MPA Stuttgart in cooperation with MAN Technology from 1992 to 2002.

The objective of the tests was to find out the strength and deformation behaviour of the booster under conditions as real as possible and to prove that there is sufficient safety against failure. Additionally, the elastic-plastic finite element method calculations could be verified and eventually calibrated.

The tests were carried out in the underground test pit (KPH2) of MPA Stuttgart, Fig. 11. The total height of the test pit is 32 m with a diameter of 14 m. The foundation is designed as work-holding area. The surrounding wall is provided with 32 fixing elements for lateral forces of ±5MN each. The test pit contains both water as well as oil hydraulic infrastructure.

During the first two tests the most significant mechanical loads which have an impact on the booster during the start and flying phase were simulated. These loads are internal pressure, thrust and reaction forces in connection with locking the booster to the main stage. These quasi-static loads were individually applied as well as superimposed. Water which was heated up and processed was used as internal pressure medium. The simulation of the vertical and lateral loads as well as the lateral thrust of the nozzle was carried out using servo-hydraulic actuators, Fig. 11. The main dimensions of the test vessels were equal to the sizes of the present Ariane 5 solid propulsion booster.

The last two tests were performed with model vessels having diameter and wall thickness equal to the dimensions of the booster. However, their length was reduced to 6 m. The model vessels contained all design features of the booster such as round seams and clevis-tang lockings. These tests were performed finally to optimise and prove the quality of the structure. Only internal pressure was used for loading. Due to the successful verification of the finite element calcula-

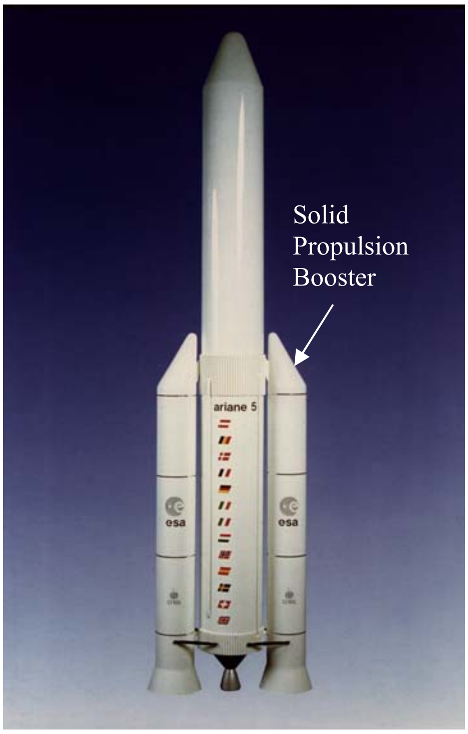

Booster data:
Total length: 25 m
outer diameter: 3.1 m
cylinder wall-thickness: 8.2 mm
low-alloy heat-treatable steel, R_m>1500 MPa
7 cylinders, 2 domes,
manufactered by flow forming and
connected by circumferential welds
as well as by positive lockings
(clevis tang connection)
Housing mass 19.6 t,   Fuel mass 230 t
max. working pressure 64 bar

Fig. 10: Ariane 5 launcher.

tions by the first two tests, it was possible to simulate numerically the superimposed external loads.

For all four tests close-to-reality loading profiles were defined. They were transferred to the test vessels by the actuators and, in case of the internal pressure loads, by the volumetric flow of the processed water as pressure medium. Nearly all pick-ups were redundantly applied.

The burst behaviour of the tested vessels is exemplified in Fig. 12 and Fig. 13. In one case large fractured area in circumferential direction can be observed, Fig. 12,whereas in the other case the failure started at the centre of the dome top and propagated longitudinally towards the dome centre bottom, (Fig. 13). The latter failure can be attributed to the internal pressure loading (burst pressure 135.6 bar) with its maximum stress in circumferential direction. The fracture running partially in circumferential direction of the vessel in Fig. 12 (fracture length 15 m) may be due to the axial thrust loads of 10 MN, which were superimposed to the internal pressure (burst pressure 91 bar).

In any case, prior to final instability large plastic extensions of the vessel diameter took place with the positive clevis tang locking acting like a corset, Fig. 13. Accordingly, an exponential increase in the hoop strain could be recorded as function of the internal pressure after the beginning of the yielding of the vessel shell, Fig. 14 (left).

The burst pressures obtained experimentally as well as the strains of the vessels corresponded closely to the pre-calculated values, Fig. 14. In the case of the vessel in Fig. 13 (final qualification test) the burst pressure was 135.6 bar and the calculated pressure was 133.3 bar. The required "Ultimate"-pressure including all pre-defined safety factors was set to 113.8 bar.

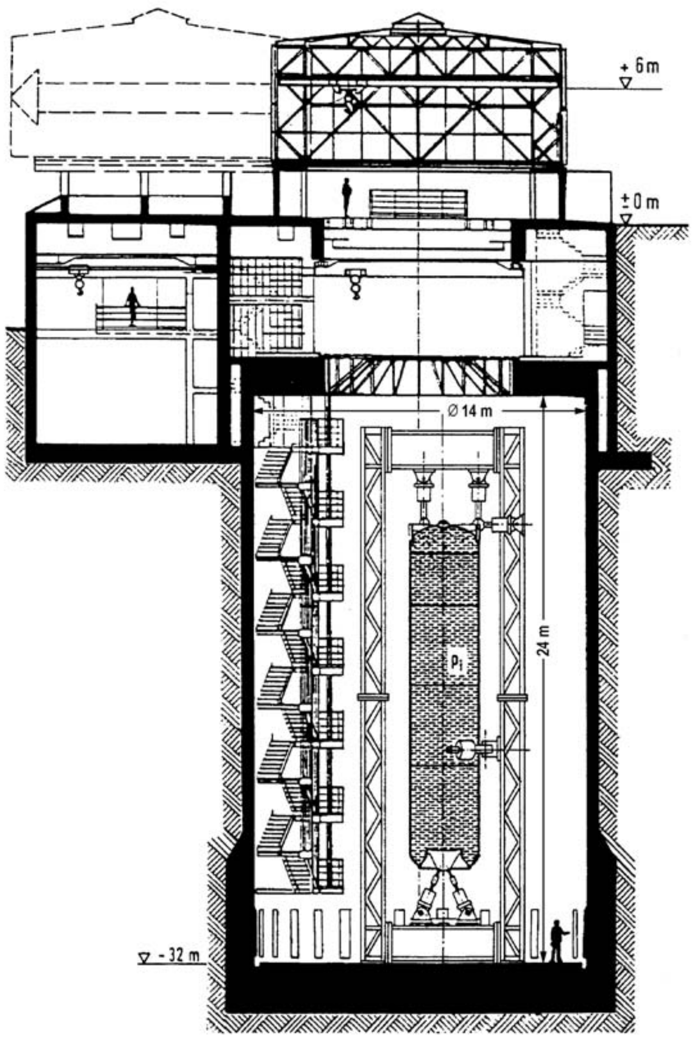

Fig. 11: Underground test pit of MPA Stuttgart with Ariane 5 test booster.

Fig. 12: Test booster loaded by internal pressure (91 bar) and axial loads of 10 MN after fracture.

Fig. 13: Test booster loaded by internal pressure (135.6 bar) after fracture.

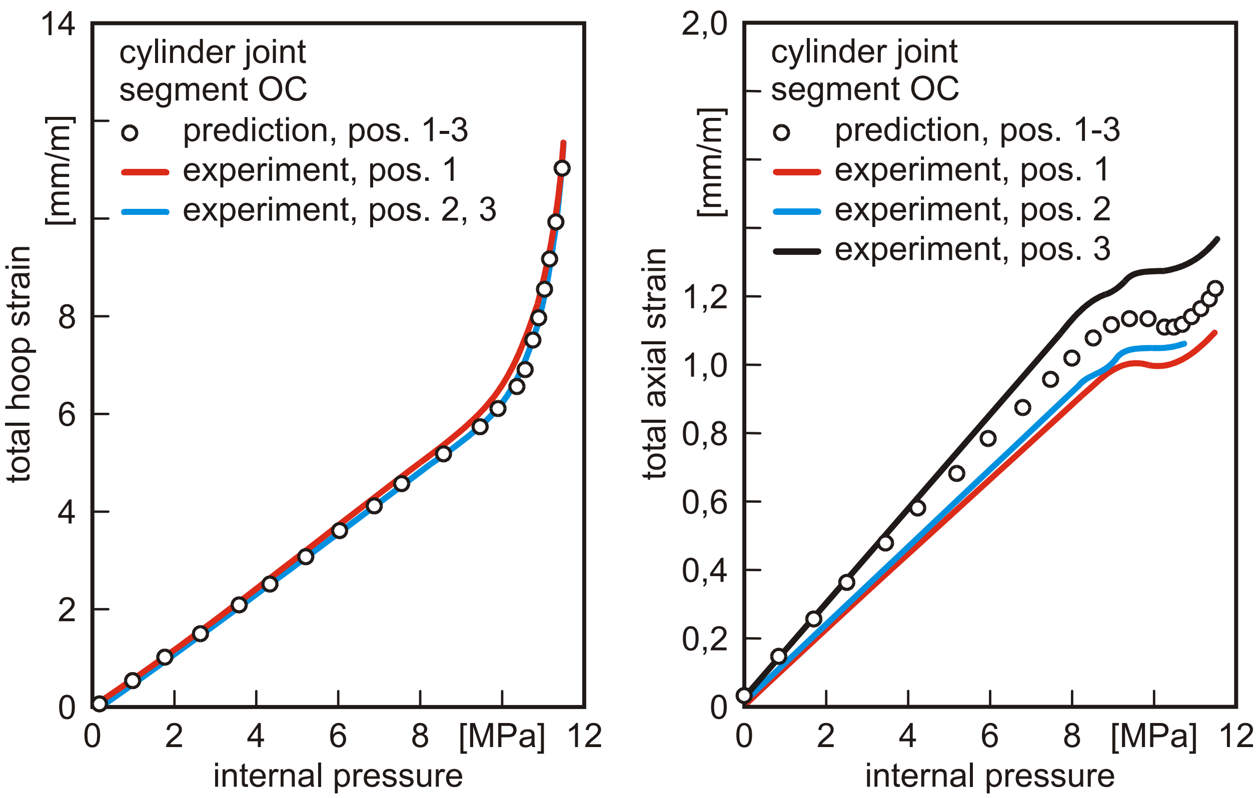

Fig. 14: Typical example of a comparison of measured local strains and the results finite element calculations.

3 FATIGUE AND FRACTURE OF FUSELAGE PANELS AND JOINTS

3.1 Effects of Tear Straps on Crack Propagation in Curved Fuselage Panels

B. Schmidt-Brandecker (Airbus-D) and M. Semsch (IMA)

The TANGO (Technology Application to the Near-Term Business Goals and Objectives of the Aerospace Industry) project represents an integrated approach for the validation of advanced technologies by designing, manufacturing and testing of major airframe components, i.e. a composite lateral wing box (including a metal to composite joint), a composite center wing box, a composite fuselage section and an advanced metallic fuselage section. It is funded in part by the European Community within the 5th Framework Programme.

In the context of the TANGO project a test on a curved fuselage panel, which is representative of the crown panel of a twin aisle commercial aircraft in the area aft of the wing, was carried out. The curved panel is 3.7 m long and 1.8 m large and consists of an aluminum alloy skin, extruded frames and stringers and bonded fiber-metal-laminates straps.

The structure was tested in the test facility for large curved panels at IMA Dresden described in the 1999 German Review, Fig. 15. Artificial damages (saw cuts) were introduced in the structure prior to the start of fatigue loading. The applied loading consisted of internal pressure and a flight-by-flight loading program representing the bending moment of the fuselage. The crack growth under the simulated flight loading was continuously monitored by optic methods.

The results of the crack propagation test suggest a significant influence of the straps, Fig. 16. The use of fiber metal laminate straps increases the damage tolerant behavior of the structure, by decreasing the crack growth rate in the skin. This behavior gives opportunities for the optimization of the design process with respect to a more damage tolerant structure.

Fig. 15: IMA test facility (left) for curved fuselage panels (right)

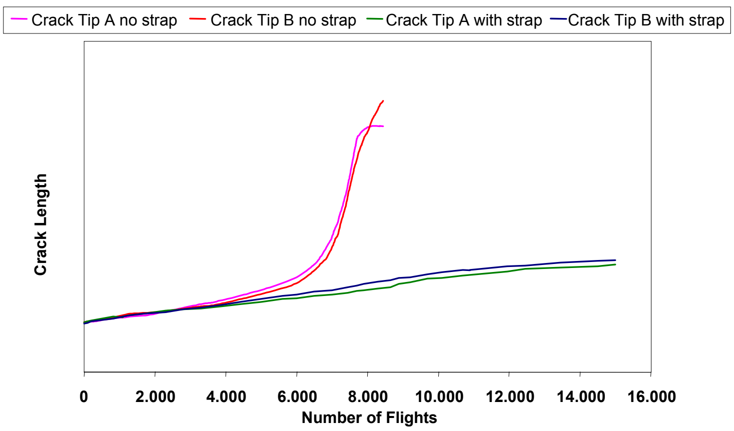

Fig. 16: Influence of a fibre metal laminate strap on the crack propagation.

3.2 Fatigue Tests with Riveted Joints

Wolfgang Fessenmayer (IMA)

Within the scope of the EU 5th Framework programme IARCAS ("Improve and assess repair capability of aircraft structures") riveted joints have been tested to determine their behaviour in case of repairs. In this connection IMA GmbH Dresden carried out fatigue tests to establish S/N-curves for different riveted joints on behalf of Airbus Deutschland, Dept. Materials and Processes, Bremen. For these tests a servo-hydraulic test rig (F_{nom} = 160 kN) with special clamping devices was used, Fig. 17. The results show the influence of different riveting techniques on the fatigue behaviour.

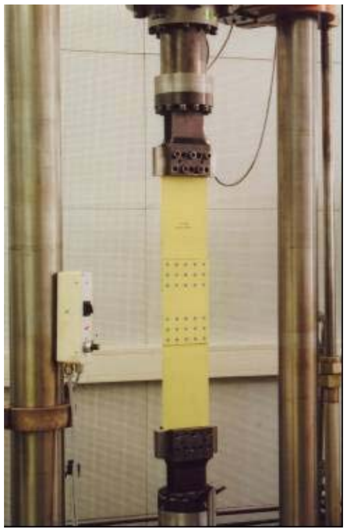

Fig. 17: Test rig with mounted riveted specimen.

3.3 Scatter in GLARE®

Thomas Beumler and Heiner Stehmeier (Airbus-D) in Cooperation with Delft University of Technology

The application of GLARE® as structural material on the A380-800 aircraft requires an investigation on both, the crack initiation and the crack propagation material scatter. Certification of the structure will be supported by the full scale fatigue specimen, which contains conventional and GLARE® materials. Preferably all structural materials should have the same scatter in order to justify the same fatigue life.

The crack initiation scatter in GLARE® is linked to the material properties of the aluminum alone, since the fibers do not carry a significant portion of the fatigue load in a non-fatigued condition. The fatigue crack propagation rates are dependant on the aluminum properties, but also on the crack bridging and delamination resistance properties.

Scatter analyses have been performed in two steps. Delft University and the NLR conducted tests with open hole specimens, which are relatively simple to inspect. A clear trend indicated lower or equal crack initiation scatter and crack propagation scatter in the aluminum layers of GLARE, compared with monolithic 2024T3 material. The same trend was observed for crack propagation scatter in open hole specimens.

In a second step riveted joints according to Fig. 18 (left) have been investigated. The fatigue critical locations are the mating layers of the GLARE2B-7/6-.4 butt strap in the two center rivet rows. So far, crack initiation and crack propagation at the mating surface layer could be detected and monitored by trial and error disassembly of the specimens and subsequent eddy current inspection, only . In order to avoid this time consuming procedure, Airbus used crack wire foils with the dimension of 25.4 mm x 5.1 mm. Each foil contains 20 parallel wires with a distance of 0.25 mm from one to the other. Up to three foils can be bonded between two bore holes. The right part of Fig. 18 shows all crack wires bonded on the mating surface of the butt strap of a particular specimen. The crack wires provide electrical signals when failing due to crack opening. The signals and the associated number of load cycles are recorded during the test. As a result crack propagation curves of high accuracy are obtained. The used crack wires possess a strain area of ±1.5% and an accuracy of ±2%.

In order to prevent destruction of the measurement device due to clamping of the sheets, one aluminum layer of each mating skin part has been milled away. The skin sheets and the butt strap sheets have been jointed with DAN7-6-6 fasteners, dry installed, but a sealant has been applied between the sheets outside the crack wire measurement locations.

Fig. 19 contains the crack propagation plot obtained from three crack wire foils which are located between two bore holes. The fatigue crack propagation rates are constant, as usual for GLARE® structures. This circumstance allows a reliable fatigue life calculation for a pre-defined crack length, if small cracks can not be detected. However, the transition point from crack initiation to crack propagation is the order of magnitude of 1 mm to 2 mm, since this is the fatigue crack length at which crack bridging becomes effective. Crack initiation scatter analysis have been performed with all available specimens related to a fatigue crack length of 1 mm. It turned out, that the crack initiation scatter is similar as in monolithic structures (results obtained from literature).

Crack propagation rates have been further analyzed for the determination of fatigue crack propagation scatter. In any case, the scatter is lower than known from monolithic 2024-joints.

Identical specimens have been used by Delft University for the establishment of a crack initiation SN curve for the mating aluminum layer of the GLARE2B butt strap. Specimens have been disassembled after pre-defined numbers of fatigue cycles by trial and error. It is observed that the absolute crack initiation life of the 'crack wire' specimens is lower compared with the 'trial and error' specimens. The effect is explained by the local influence of the milling of the skin sheets which belong to the 'crack wire' specimens.

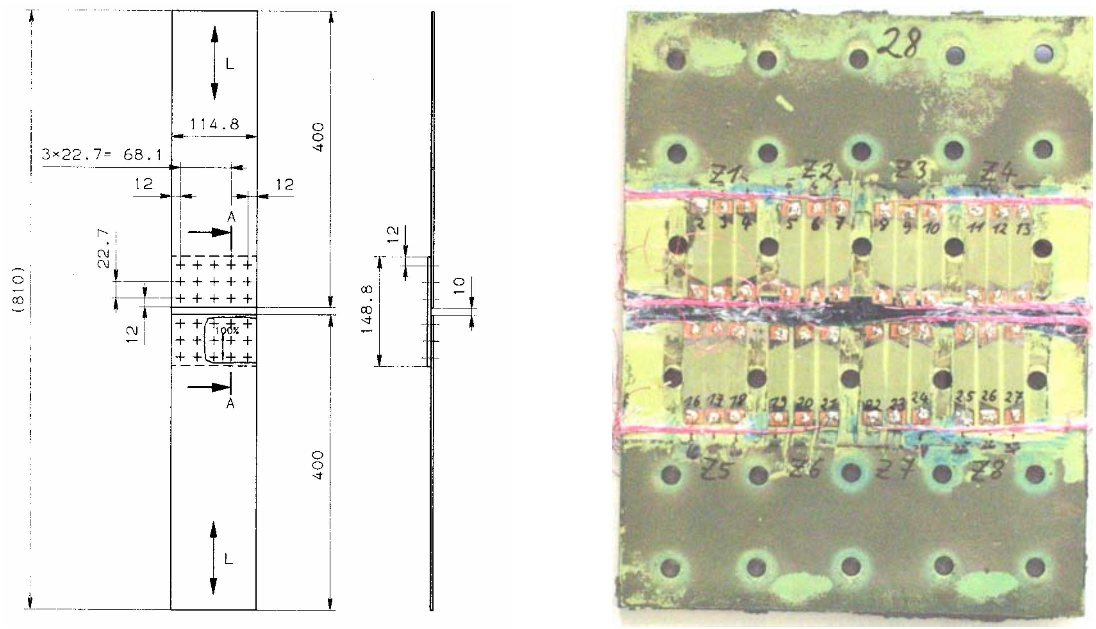

Fig. 18: Specimen configuration (left) and crack wire foils bonded on the mating surface of the butt strap of a specimen (right).

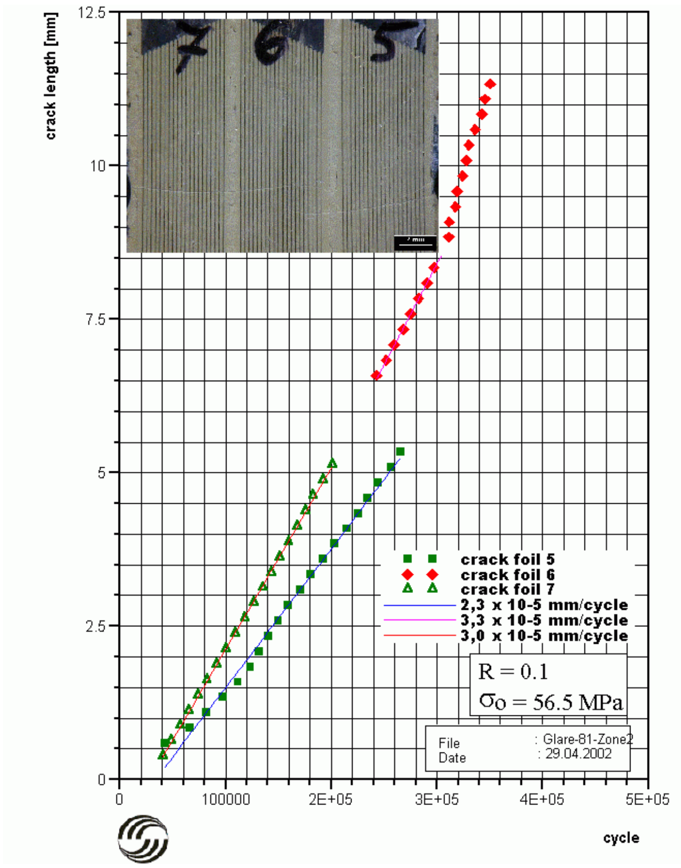

Fig. 19: Crack propagation versus cycles obtained from three crack wire foils which are located between two bore holes.

4 FATIGUE AND FRACTURE OF WELDED JOINTS

4.1 Damage tolerance tests of plane integral panels

M. Lieback, M. Scheffler and R. Franke (IMA)

The national program AIR (aluminium integral fuselage) includes damage tolerance tests of plane stiffened panels. The panels consist of an aluminium skin with laser beam welded stringers. More than 45 panels with different design and manufacturing principles were tested in the servohydraulic test facility at IMA Dresden, Fig. 20.

The crack growth of the panels was investigated under pulsating tensile stress. Two scenarios starting from a saw cut of the type "crack above a broken stringer" were tested. The first type of tests was completed with a two bay crack residual strength test. The second test was stopped after the failure of adjacent stringers during the fatigue cycling.

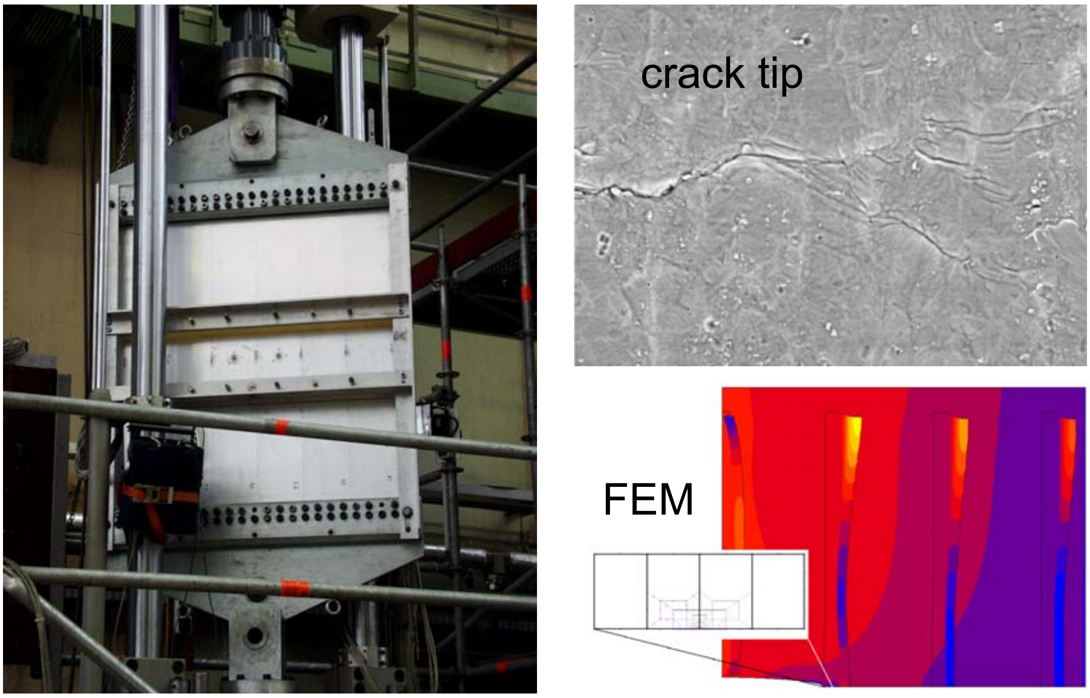

Fig. 20: Fatigue and residual strength tests and analysis of integral fuselage panels at IMA.

4.2 Replacing Riveted Longitudinal Splices in the Pressurized Fuselage by Friction Stir Welded Butt Joints

Marco Pacchione (Airbus-D)

In the continuous effort to improve the structural efficiency of primary structures, Airbus is working on the development and introduction of new and innovative technologies. After the introduction of Laser Beam Welded (LBW) stringers in the lower shell of A318 and A380, other applications of welding are investigated. It is generally recognized that welding can provide cost savings compared to riveted joints, but the traditional fusion welding processes (TIG, MIG and Laser Beam) can be applied only to a limited range of aluminium alloys (6000 series) and always with a detrimental effect on the mechanical properties.

Friction Stir Welding (FSW) is a solid-state welding process, which can weld aluminium alloys (similar or dissimilar) that conventional welding methods cannot, and delivers mechanical properties that are generally higher than the ones of other welding processes. FSW technology is expected to deliver manufacturing cost reduction and also performance benefits (weight reduction) due to higher allowables, possibilities of design optimisation and parts number consolidation; candidate FSW applications have been identified for both fuselage and wing primary structures.

One promising application for FSW is the replacement of fuselage longitudinal splices (typically 3 rows of fasteners) in shell and super-shell manufacturing with welded butt joints. In contrast, the FSW application in the final assembly of the fuselage barrels for the joining of supershells is considered problematical because of complex tooling and very strict manufacturing tolerances. From the production point of view the main opportunities are related to the reduced numbers of parts and assembly stations, easy automation, no sealing requirements. From the design point of view the absence of fastener holes improve the fatigue behaviour and avoid the issue of Multiple Site Damage (MSD).

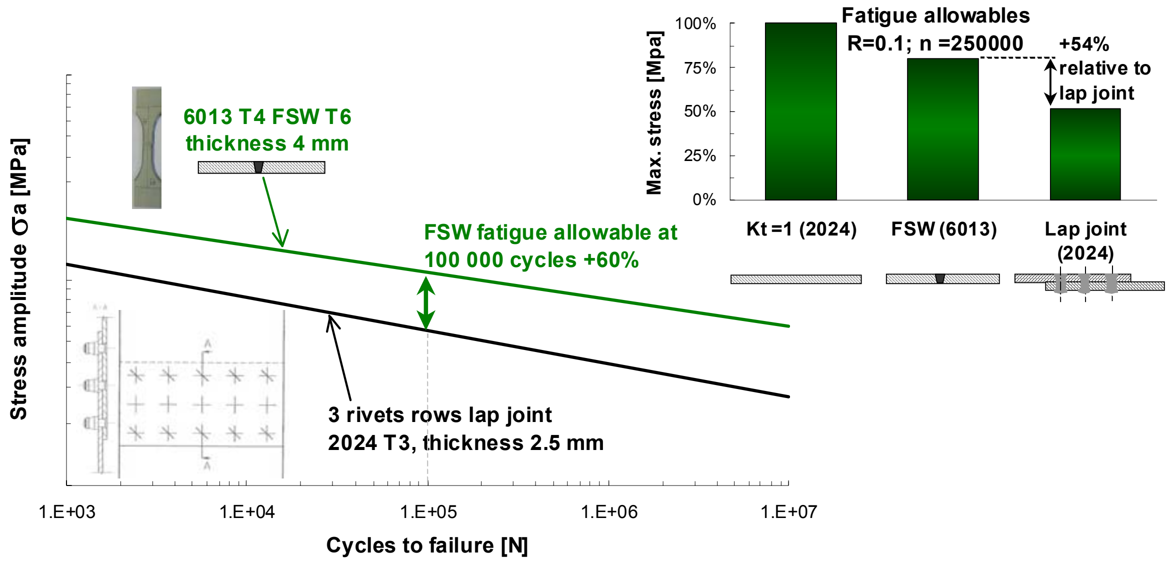

Fig. 21: Comparison of fatigue curves for 2024-T3 riveted lap joints and 6013 Friction Stir Welded butt joints with skimmed surface and implications on fatigue allowables (data from D. Lohwasser, Airbus-D Bremen).

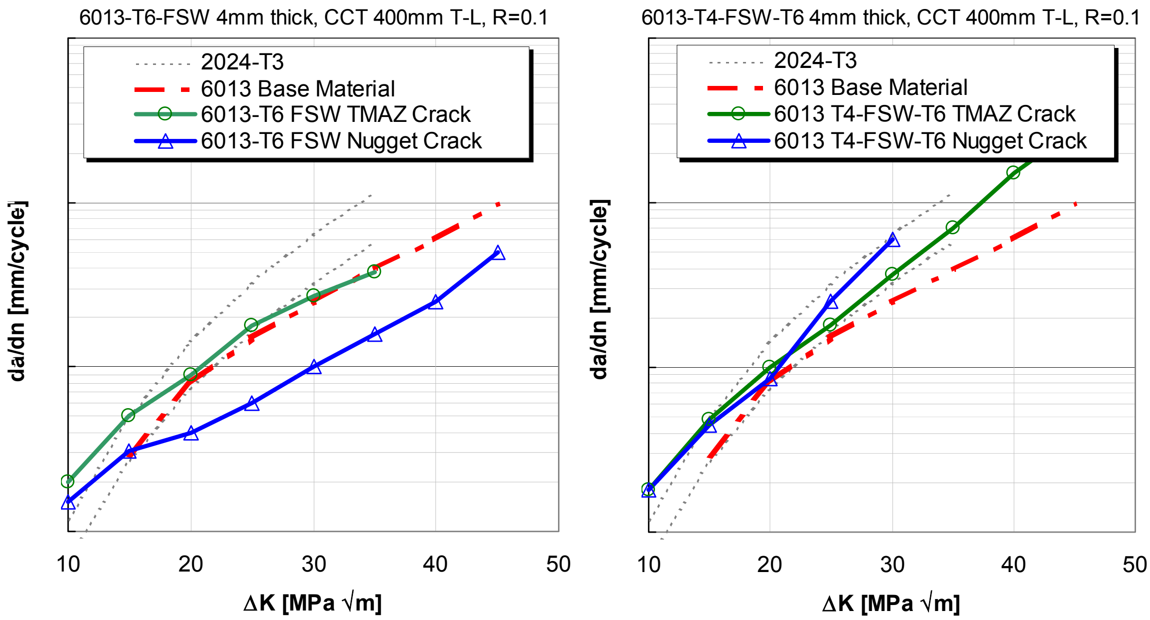

Fig. 22: Comparison of crack propagation rate for 6013 base material and welded in two different heat treatments: T6 as welded and T4 post treated to T6 condition. 2024-T3 is included as reference material. Cracks were propagated in the nugget and in the thermo-mechanically affected zone (TMAZ) of CCT specimens (data from D. Lohwasser, Airbus-D Bremen).

The main structural load for the longitudinal welded joints are given by the pressurization loads and the main failure scenario is a longitudinal crack running parallel to the weld line: in the nugget or close to it. The longitudinal configuration of the welded joints limits the impact of the presence of welding on the crack propagation properties of circumferential cracks due to the reduced size of the area affected by the welding. However, the integral nature of the resulting skin will reduce the crack stopping capability inherent of riveted joints.

To comply with the current fatigue and damage tolerance regulations for large transport civil aircraft the main structural criteria which have to be fulfilled by a fuselage welded joint are:

- Durability (fatigue, crack initiation, no MSD);
- Damage tolerance (slow crack propagation);
- Residual strength (high toughness, crack arrest capability);

- Large damage capability (2 bay crack).

In the frame of TANGO European research project several coupons and panels tests have been carried out to determine the mechanical properties of FSW butt joints. A comparison of the fatigue life for traditional 3 rows of rivets lap joints and 6013 FSW butt joints is given in Fig. 21. Considering an aircraft with a design service goal of 50 000 flights and a fatigue scatter factor equal to 5 the resulting design fatigue life is 250 000 cycles. As shown in Fig. 21 the maximum stress fatigue allowable for a FSW joint could be 50% higher than a comparable riveted lap joint.

The crack propagation parallel to the weld nugget has been investigated for the 6013 and the test results confirmed the already known influence of heat treatment on the da/dN curves. Despite a large scatter which depends on the crack location (centre of the nugget vs. heat affected zone) the test data is encouraging. The crack propagation rate for 6013 FSW is generally higher than in the case of base material but not larger than the upper scatter limit of the reference material for fuselage applications: 2024-T3. The 6013-T6 in the as welded condition has better da/dN rates than 6013-T4 post weld heat treated to T6 condition, but the latter condition shows higher static properties.

Further investigations related to the residual strength of FSW joints are currently ongoing.

4.3 Residual Stress Effects in Friction Stir Welds

Claudio Dalle Donne and Tommaso Ghidini (DLR-WF) and Anke Pyzalla (Technical University of Berlin)

Residual stress analysis on 4 mm thick friction stir welds (6013-T4) were carried out using the cut compliance technique and non-destructive diffraction methods [2]. The results of the different techniques were in good quantitative and qualitative agreement. The longitudinal stresses were always higher than the transverse residual stresses and revealed an “M” like distribution with small compressive residual stresses in the weld seam and high tensile residual stresses in the heat affected zone. Welding experiments with different tools showed that larger tool diameters widened the M of the residual stress distribution, Fig. 23. From the investigations presented and the known literature it seems that the peak tensile values of longitudinal residual stresses are in the range of 30 to 60 % of the weld material yield strength and 20 % to 50 % of the parent material yield strength.

Fatigue crack propagation tests of 4mm thick friction stir welded (FSW) joints of the aluminum alloys 6013-T6 and 2024-T3 were carried out with compact tension specimens at different mean stress levels (R-ratios) and crack orientations [3]. It was shown that residual stresses alter the applied load ratio in the welded specimens. On the basis of the effective stress intensity factor range ΔK_{eff}-approach and a simple residual stress intensity factor estimation, it was shown that the differences in the fatigue crack behavior of welded specimens and parent material (2024-T3 and 6013-T6) were almost completely caused by residual stresses and not by the different resistance to FCP of the various weld microstructures, Fig. 24.

Finally the prediction of simple overload experiments carried out with FS welded specimens using the AFGROW or the NASGRO code gave the best results if both the residual stresses and the overload effects were considered.

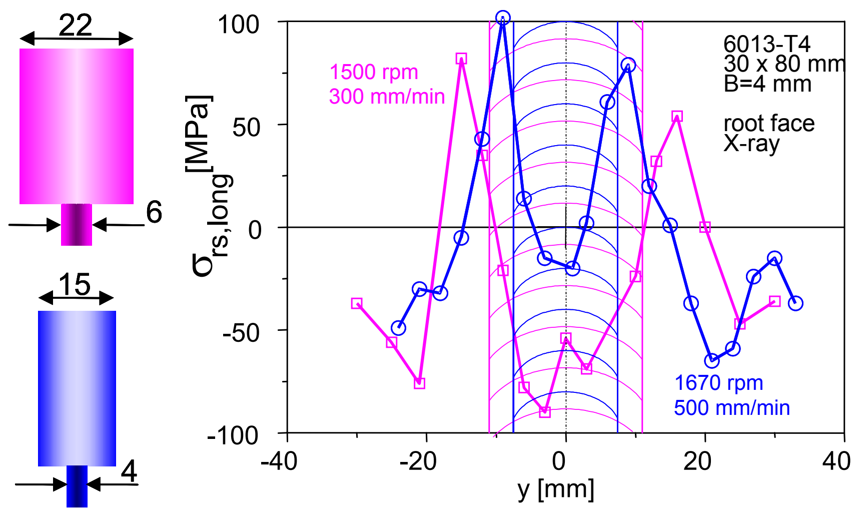

Fig. 23: Longitudinal residual stresses in 4 mm thick friction stir welds (effect of shoulder diameter).

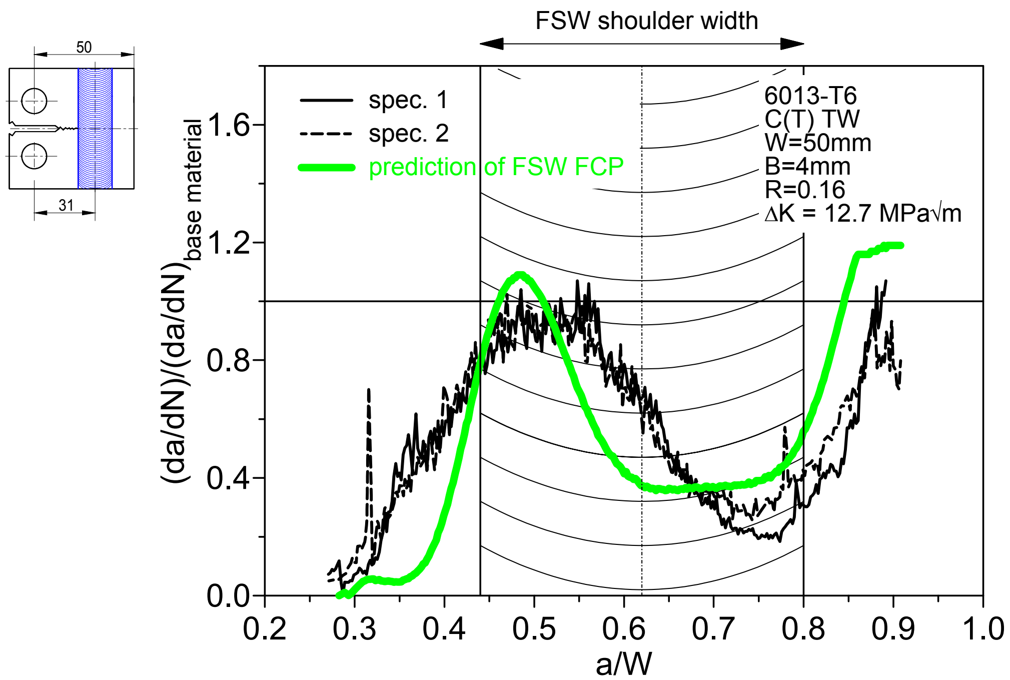

Fig. 24: Prediction of constant ΔK fatigue crack propagation perpendicular to the weld using base material ΔK_{eff}-data and the residual stress distribution in the specimen.

4.4 Effect of Heat Treatments on Mechanical Properties of Friction Stir Welded 6013

Claudia Juričić, Claudio Dalle Donne and Ulrike Dreßler (DLR-WF)

The effect of pre and post FSW heat treatments on hardness, tensile strength, fatigue crack propagation and fracture toughness of 4 mm thick sheet of 6013 (unclad) was investigated [4]. Following heat treatments were considered:

- FSW in T6 and post-weld natural aging
- FSW in T4 and post-weld heat treatment to T6
- and finally FSW in T6, subsequent re-aging to T6

Friction stir welding generally caused a decrease in strength and hardness in the heat affected zones, which could not be recovered by the simple pre and post heat treatments investigated here. If only strength is required, welding in T4 and subsequent aging to T6 is the most appropriate procedure, since over 90 % of base material yield and ultimate strength was obtained for this combination. Welding in T6 and natural aging gives the most damage tolerant weld microstructure with the disadvantage of a lower tensile strength. It is not recommended to use the T6 FSW T6 combination, because of the very narrow low hardness region in the HAZ, which decreases strength and may lead to low toughness failure if a crack is located in this low hardness band.

4.5 Fatigue Behaviour of Welded Aluminum under Multiaxial Stress States

M. Kueppers and C.M. Sonsino (LBF)

Fatigue critical areas of many structures are subjected to multiaxial states of stress and strain. They do not only result from local constraints in notches but can also be caused by multiaxial external loading, for example combined bending and torsion. The most complex local multiaxial stress / strain states are those with varying directions of principal stress / strain under combined loading, so the designer is confronted with the following problems in the assessment of multiaxial stress/strain states:

- Which kind of stresses / strains (nominal, hot-spot, structural, local) should be used?
- Which hypothesis should be used for aluminium for the transformation of the multiaxial state into an equivalent one (von Mises or a modification)?

- can design S-N curves obtained under uniaxial loading be applied for the assessment of multiaxial loading?

Latest research results on welded steel joints show a loss of fatigue life for changing principal stress directions simulated by out-of-phase bending and torsion compared to constant directions given by in-phase loading. This behaviour is not predictable by any conventional hypothesis. However, the fatigue behaviour for aluminium welds is to a large extent unknown. Therefore, a research project was initiated for investigating this topic.

Base materials for the specimens have been extruded tubes and plates of the artificially-hardened alloy EN AW 6082 T6. After optimisation of the weld geometry to achieve a welding of maximum quality and to overcome problems with the interpretation of weld defects, the specimens were welded with a combination of TIG- and MIG-welding. Fig. 25 shows an overview of the critical area, the transition from the tube to the flange, as a macrosection. Tests were performed on tube-to-tube and tube-to plate specimens under pure bending, pure torsion and combined bending and torsion with in-phase and out-of-phase fully reversed (R = -1) loading.

The most interesting and important result of this work is, that experiments reveal no difference between in- and out-of-phase combined loading, see Fig. 26. The application of the conventional strength hypotheses like von Mises, Tresca or Galilei (principal stress) cannot describe this behaviour; they all predict an increase of fatigue life for out-of-phase

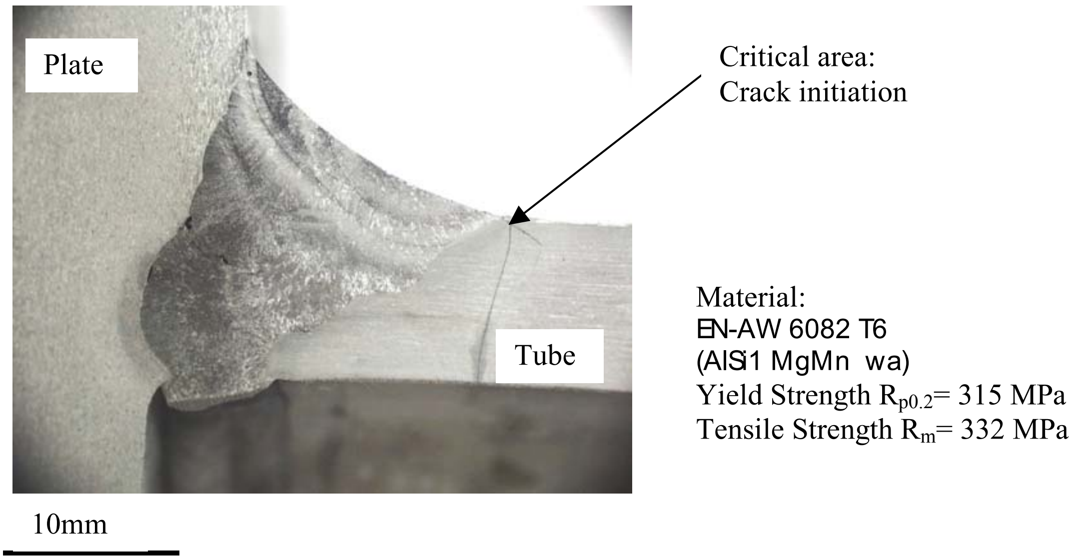

Fig. 25: Macro-section of the investigated welded specimens.

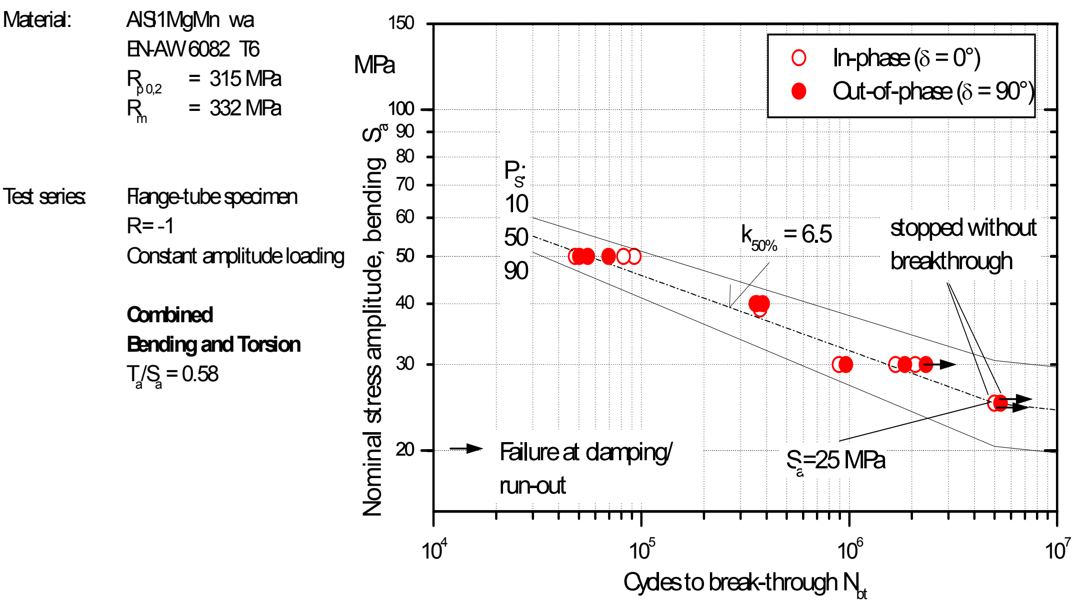

Fig. 26: Test results under in-phase and out-of-phase loading.

loading. Also new hypotheses for describing the fatigue life reducing effect of out-of-phase loading for ductile steels in the welded or non-welded material states cannot be used for welded aluminium joints. However, experiences with unwelded materials under multiaxial loading show that the behaviour can be divided into classes with regard to damage mechanisms, depending on the ductility of the material:

- Ductile materials, where damage is caused mainly by shear stresses; for such materials out-of-phase loading causes a reduction of fatigue life, as also observed for welded steel joints.
- Low-ductile (brittle) materials, where damage is caused mainly by normal stresses. Out-of-phase loading increases the fatigue life. This is appropriate for cast materials.
- Semi-ductile materials, where damage is caused by a combination of shear and normal stresses; the fatigue behaviour is neutral, as observed for steel casting and here for the welded aluminium joints.

For the description of the semi-ductile material behaviour of the investigated welded aluminium a critical plane oriented hypothesis on the basis of a combination local normal and shear stresses (KoNoS) has been developed to calculate an equivalent stress. Therefore the knowledge of the local structural stresses is necessary. It can be derived from strain gage measurements or finite-element calculations in dependency from the geometry. This approach leads to an adequate estimation of fatigue life for the tested aluminium weldings.

The authors are pleased to acknowledge the Arbeitsgemeinschaft industrieller Forschungsvereinigungen (AiF), Cologne/Germany, for supporting this work (sponsoring No. 10731), Alcan, Göttingen/Germany, for the provision of the material and specimens and the Working Group FA 9 “Construction and Calculation” of the Deutscher Verband für Schweißtechnik (DVS), Düsseldorf/Germany, for the scientific coaching of the project.

5 FATIGUE AND FRACTURE OF METALLIC FUSELAGE MATERIALS

5.1 Influence of Load Sequences on Crack Propagation of Initial Flaws

R. Buchholz (IMA)

The load sequence has an important influence on the crack propagation. To determine the influence of typical aviation load sequences on the crack propagation behavior, a number of coupon tests were performed with different load programs. The loads were typical for the lower wing surface.

Coupons made of aluminum alloy 7475-T7351 with through-the-thickness-cracks were loaded with 3 flight-by-flight load programs:

- Single steps (one load cycle correspond to one flight)
- Flight program 1 with ground loads
- Flight program 2 without ground loads

The single step test was characterized by a cosine shape with a maximal stress level of 120 MPa and a stress ratio of 0.1. The flight program 1 consisted of 87 different individual flight types with different severities. They were randomly distributed in repeated blocks of 2000 flights. Furthermore the load sequence included negative load excursion representing ground loads. The flight program 2 consisted of blocks of 4000 completely different flights. The ground con-

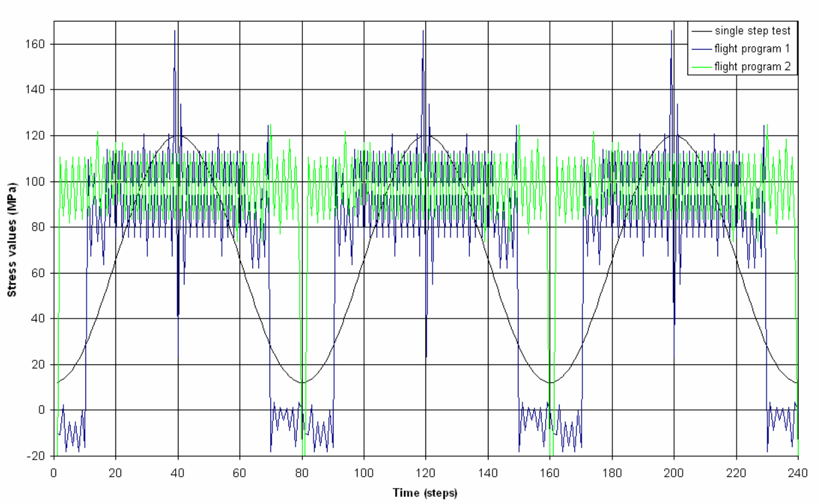

Fig. 27: Examples for load spectra (3 flights).

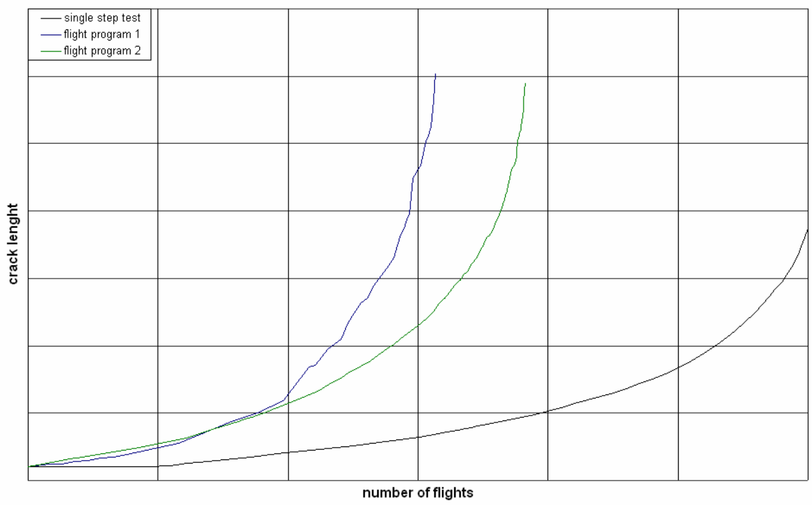

Fig. 28: Crack propagation curves of 7475-T7351 center cracked specimens.

ditions were represented by one load case per flight, Fig. 28.

The tests were performed in an uniaxial servo-hydraulic test rig controlled by a special control system. The nominal load values were generated and controlled by a separate external computer. The crack length was measured optically through a travelling microscope.

Fig. 28 shows crack propagation of the coupons subjected to different load programs. The differences of the curves are attributed to the load sequence effects. In comparison to the simple single step test simulating take-off and landing load cycles the flight programs cause higher crack propagation rates. Analytical investigations on the damaging effects of the over- and underloads as well as the intermediate smaller cycles of the flight programs are under way..

Further investigations regarding the influence of omission and truncation of load excursions are in process.

5.2 Lifetime Prediction for Aluminium 6013 in the Light of Statistical Aspects

S. Rödling (UniBw-M), I. Bazios (IABG) and H.-J. Gudladt (UniBw-M)

For lifetime predictions of random loaded structural components the characterisation of crack propagation behaviour is indispensable. Taking different material charges and differences in their microstructure into account a scatter of crack propagation data has to be noticed. Even a small variation of crack propagation curves leads to a high scatter in the calculated crack propagation lifetimes, and unambiguously, a precise lifetime prediction can only be made in the light of a statistical view of crack propagation data.

For the acquisition of crack propagation data and threshold values investigations with the load shedding method according to ASTM E 647 on SEN-specimens of aluminium 6013 T62 have been progressed. The actual crack length was continuously measured by a DC potential drop method. This permits crack propagation tests under K-controlled conditions [5, 6], where the scatter in *da/dN* is very low, compared to many other crack growth tests given in the literature.

Fig. 29 shows a measured crack propagation curve for a stress ratio $R = -1$ in ambient air. For lifetime predictions the crack propagation curve can be described by two analytical functions developed by Paris [7] and Klesnil - Lukáš [8] (solid line in Fig. 29). In these two functions there are three variables (the threshold, ΔK_{th}, the exponent, *m*, and the empirical constant, *C*, of the Paris law) which are necessary for precise lifetime calculations. The threshold has been found to be $\Delta K_{th} = 3{,}1\ MPa\sqrt{m}$. The stable crack propagation behaviour in the Paris regime can be divided in two areas with different exponents of nearly two and four, respectively. Normally, *da/dN* calculations have to be done in the upper Paris regime ($\Delta K > 10\ MPa\sqrt{m}$) and because of the magnitude of the quantified variation of *C*, this value is the leading parameter for a statistical consideration of crack propagation data. Fig. 29 shows the corresponding scatter band within the upper and lower bound.

In order to get a better insight into statistical aspects of crack propagation, all data resulting from the ΔK regime between *10* and $40\ MPa\sqrt{m}$ were transformed to a K_{max} level of $6\ MPa\sqrt{m}$ [9]. The density function of these data obeys a log normal distribution as it has been shown in Fig. 30. In this figure the quantity $P_{Ü}$ *(da/dN, K=const)* is plotted against *log da/dN* by using a log normal probability net and the assessor of Rossow [10]. If the density function and the corresponding assessor fit quite well, all data follow nearly a straight line as it can be seen in Fig. 30. The scattering parameter $T_N = (P_Ü = 0{,}1) / (P_Ü = 0{,}9)$ can be used as a quality criterion for precise lifetime calculations. Values higher than $T_N = 1{,}56$ as it has been calculated in the presented case, are leading to a more pronounced scatter band and, therefore, to stronger uncertainties in the lifetime prediction.

In case of load sequences with two different stress amplitudes the overload cycles lead to a temporary deceleration of the crack propagation rate [6]. The latter has been taken into account by using a modified crack propagation model after Wheeler [11]. The calculation was made for a test with a constant stress level $\sigma = 60\ MPa$ and two single overloads with an advantage factor of 2,5 (150 % overload). Fig. 31 shows the model calculation in the *a(N)* vs. *N* presentation. By using the scatter of the *da/dN* data, an upper and lower bound has been calculated for the *a(N)* curve that contains the two

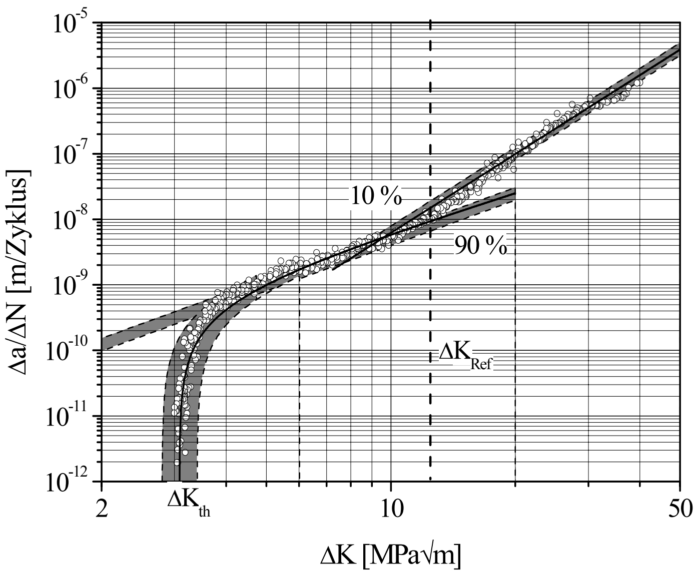

Fig. 29: Crack propagation data and its scatter plotted within an upper PÜ = 10 % and lower PÜ = 90 % bound.

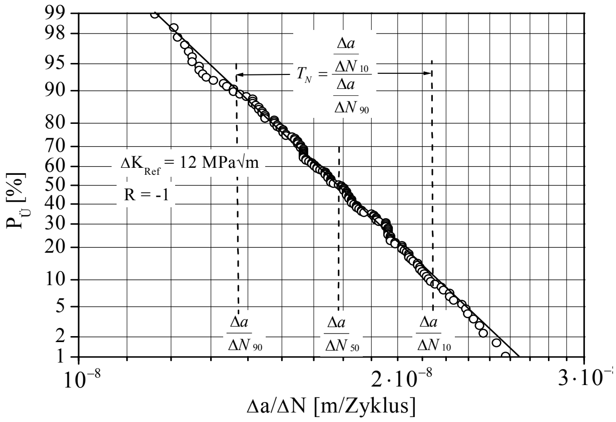

Fig. 30: Log-normal distribution of crack propagation data presented in a probability net. The quantity $T_N = (P_Ü = 0{,}1) / (P_Ü = 0{,}9)$ has been used for the scatter band in Fig. 29 and Fig. 31.

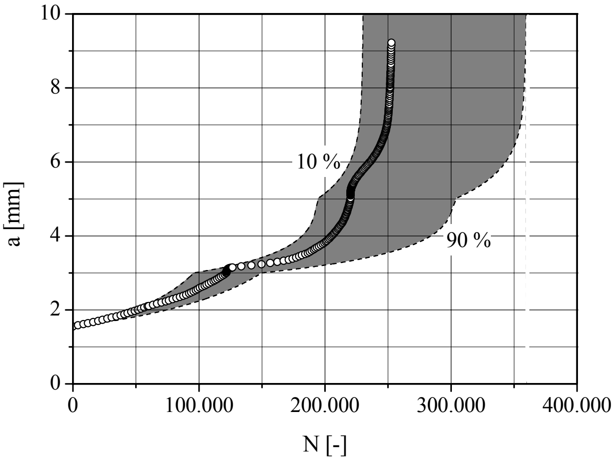

Fig. 31: Lifetime predictions by using the scatter from

continuously measured during the fatigue test

overloads. As an example experimental data have also been plotted in this figure and the good correlation between these data and the model calculation is clearly visible.

In realistic cases it should be noticed that the scatter of crack growth rates increases in a significant manner compared to those results given in this paper. Consequently, all selected model calculations have to be proved in the light of these statistical aspects.

5.3 Short crack growth in Al 2524-T351 and Al 6013-T6

Andreas Tesch, Hubert Döker, Karl-Heinz Trautmann (DLR-WF) and Concepcion Escobedo (Airbus-D)

In a joint research project of AIRBUS Deutschland in Hamburg and the Institute of Materials Research of the German Aerospace Centre (DLR) in Cologne reliable basics should be prepared to design structural elements in a safe and economic way considering the Initial Flaw Concept. This three-year project, which started in January 2002, includes the following points:

- Literature study on the crack growth behaviour of short and small cracks
- Characterisation of the materials (tensile tests, da/dN- ΔK curves at different R-ratios, thresholds for crack growth, both for long cracks)
- Investigation of the behaviour of short and small cracks emanating from a rivet hole (influences of different R-ratios, residual stresses, loading spectra) [1]
- Investigation of the behaviour of short and small cracks emanating from a rivet joint
- Modelling the short and small crack behaviour and generating an analytical computer code to predict the lifetime

The goal of the project is to develop analytical tools to calculate the crack growth of short and small cracks in structures.

Up to now characterisation tests with long cracks have been performed. For both materials the results of the tensile tests lay in the permitted scatter band according to the Airbus Standards. The crack growth tests were performed according to ASTM E647 with M(T) specimens under computer control on closed loop servo-hydraulic testing machines at room temperature in laboratory air. The load wave form was sinusoidal at a test frequency of 10-50 Hz and adapted to the crack growth rate.

[1] According to ASTM 647 appendix X3 a crack is defined as being ***small*** when **all** physical dimensions are small in comparison to a relevant microstructural scale, continuum mechanics scale or physical scale. The specific physical dimensions that define ***small*** vary with the particular material (e.g. grain or particle size), geometric configuration, and loadings of interest. A crack is defined as being ***short*** when **only one** physical dimension (typically the length of a through-crack) is small according to the description above.

During the tests the crack length was monitored by the DC (direct current) potential drop technique. Additionally, the tests were stopped after a certain crack propagation and the crack length at the surface was measured with an optical microscope. For some specimens markers were set on the fracture surface during the test by changing the R-ratio. The corresponding crack lengths were measured after the tests and compared with the results from the DC potential drop technique and the optical surface measurements. Due to the small thickness of the specimens no significant difference could be seen. Therefore, this very time consuming procedure was not applied for all specimens.

The da/dN-ΔK curves showed the expected, typical sigmoidal curves, shifted from higher to lower stress intensity ranges as the load ratio R is increased (e.g. Fig. 32 for Al 2524-T351). The specimen orientation has no influence on the crack growth behaviour in these materials (see Fig. 33).

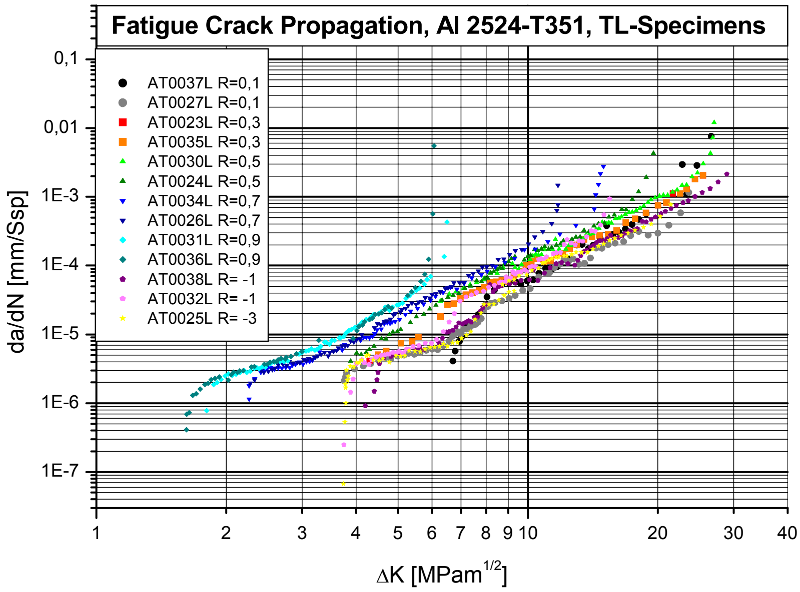

Fig. 32: da/dN- ΔK curves for different R-ratios for the material Al 2524-T351

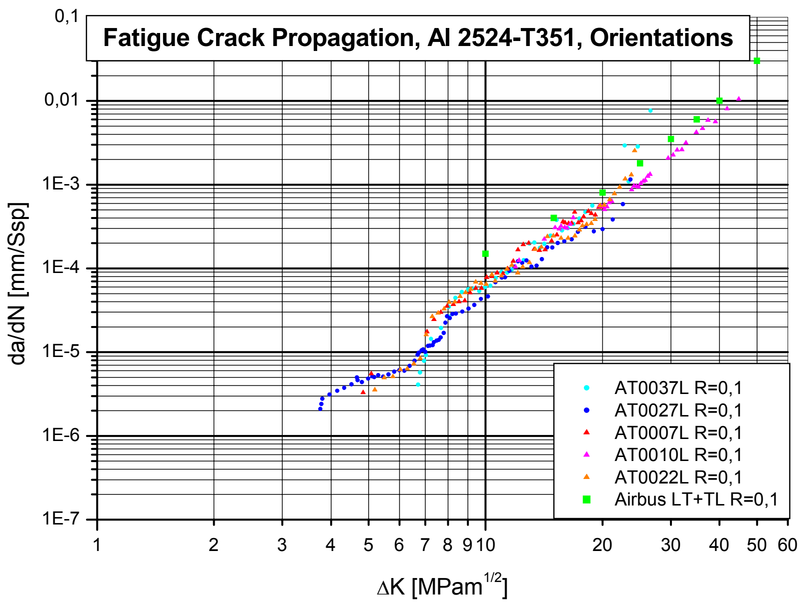

Fig. 33: da/dN- ΔK curves for different specimen orientations for the material Al 2524-T351 (Specimens: AT0007L-22L are LT, AT0027L and 37L are TL-oriented)

6 FATIGUE AND FRACTURE OF COMPOSITES

6.1 Numerical Investigations on GLARE

S. Hinz and K. Schulte, TU-HH

GLARE® is a fibre reinforced metal laminate (FML), consisting of thin metal sheets of aluminium alloy 2024-T3 (GLARE 1: Al 7075-T761) with thicknesses between 0.2 and 0.5 mm, which are cured together with S-glass reinforced epoxy prepregs with a nominal thickness of 0.125 mm and different lay-ups. Because of the presence of the fibres between the metal layers, the growth of fatigue cracks is strongly diminished compared with monolithic aluminium alloys and crack initiation is also delayed. This and weight savings of about 20% are the main reasons why GLARE is chosen for fuselage sections of the new large aircraft A380 by Airbus [13].

The several GLARE® grades differ substantially in their lay-ups of the glass fibre reinforcement. E.g. GLARE 2 consists besides the metal layers of unidirectional orientated glass fibre layers, while GLARE 3 is reinforced with cross-ply prepregs (Fig. 34). Thus, the material shows an anisotropic elastic behaviour combined with non-linearities when deformation of the metallic fraction reaches the plastic region. Moreover, the behaviour of the material is influenced by residual stresses from the curing process.

Of special interest in this project is the damage behaviour of the FMLs. The mechanical damage development in GLARE® is mainly dominated by two damage types: delamination between the fibre reinforced epoxy and the metal layer and cracking or plastic deformation of the metal layers until failure occurs in the transverse reinforced fibre layers. The effective damage mechanisms depend on the applied load and are, as for composite materials in general, of complex nature. Thus, attempts had been made to describe the damage behaviour of GLARE® with numerical methods.

The aim of the project is to achieve a better understanding of the fracture behaviour of GLARE® in detail, to analyse the variation in mechanical properties caused by the damage development for a large-scale FEM model and to verify the material properties considering aspects of damage tolerance. A successful modelling finally leads to a reduction of necessary tests of the material itself and of structural components and thus to cost savings for the aircraft industries.

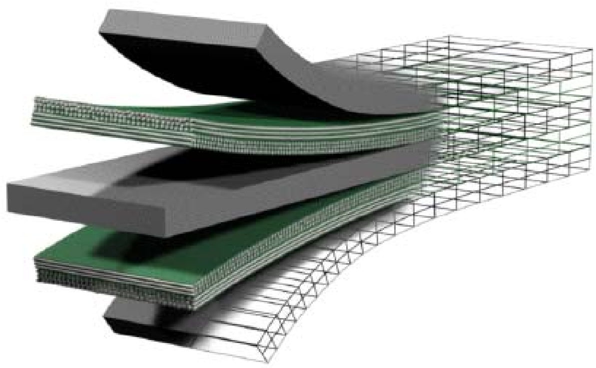

Fig. 34: Schematic structure of cross-ply GLARE 3-2/3-0.3 and mesh with finite elements [14].

At TU-Delft computational methods have been developed to simulate the damage development in GLARE®. The material has been modelled in a mesoscopic scale, which means that phenomena like matrix cracks and interface failure between fibres, matrix and metallic layers are generalized on a level of a single layer of the laminate. To model the crack growth between the layers, solid-like shell elements and corresponding interface elements had been introduced [15]. This allows to model the separation of delaminated layers controlled by a damage array d_{ii} and thus, to model the change in mechanical properties as a result of the progression of damage [12]. The effect of this damage array d_{ii} depends on the choice of the values for the implemented material parameters; in this case the fracture toughness G_{1C}, which describes the energy, needed for creating the fracture surface (Fig. 35). With this model local buckling in combination with delamination growth could be modelled [12].

To get a better understanding of the fracture process, the implementation of physically based parameters into the model is helpful. To get the amount of energy G_{1C} that is used to create the fracture surface without counting the dissipated amount of the applied work, tests with quantitative measures of the released energy could be useful. E.g. the amount of applied work, which is dissipated into thermal energy, will be determined by using the infra-red camera technique in an appropriate test (e.g. SCB test).

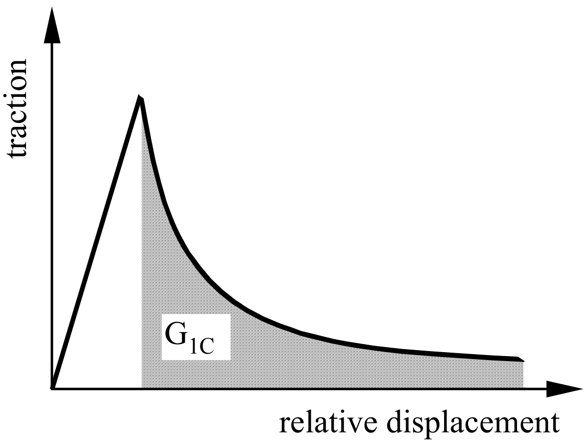

Fig. 35: Traction - relative displacement relation in mode I direction for the damage model [12].

6.2 Moisture Diffusion in GLARE®

Thomas Beumler (Airbus-D) in Cooperation with Delft University of Technology

The application of Fiber Metal Laminates like GLARE® as structural material for civil aircraft requires an understanding of environmental influences on both, material properties and design allowables. An epoxy based prepreg system has been qualified for a GLARE®–type which is applied on the A380-800 aircraft. In addition to environmental effects which are considered for monolithic aluminum, e.g. corrosion, effects on the bonding properties between resin and fibers and between resin and metal due to moisture absorption need to be investigated for Fiber Metal Laminates.

The absorption path in GLARE®, however, is different compared with pure composite structures. Due to the barrier function of the aluminum sheets moisture penetration is limited to the sheet edges and to bore holes, Fig. 36. The diffusion rates are dependant on the fiber orientations in the prepreg. Since the fibers in GLARE2, GLARE3 and GLARE4 are always oriented parallel and/or perpendicular to the rolling direction of the aluminum, the situation is relatively simple at the sheet edges. A calculation of moisture concentrations around bore holes is more complicated, since the fiber orientation changes continuously along the bore hole edge.

A systematic investigation of the problem is under evaluation in cooperation with Delft University of Technology. The sequence of the program is listed below (for GLARE3, other types are considered in parallel programs):

1. Perform weight gain tests with rectangular specimens (accelerated ageing, constant climates) for validation
2. Evaluate a one-dimensional diffusion calculation method
3. Perform weight gain tests with open hole specimens.
4. Provide a numerical solution for the prediction of iso-concentration lines around bore holes for specimens exposed in a constant climate.
5. Expose open hole GLARE® specimens outdoors and perform weight gain measurements.
6. Relate the outdoor exposure results to the evaluated calculation method and predict the moisture concentration around bore holes for 30 years aircraft service.
7. Relate static and fatigue properties of the material to the predicted moisture concentration.

Items 1) and 2) are discussed in this paper. Weight gain measurements with GLARE® require a careful definition of the specimen shape, since the aluminum sheets contribute significantly to the absolute specimen weight. The specimens should be as small as possible in order to get use of the common measurement range of a balance. Rectangular specimens with the sizes 60mm x 40mm and 100mm x 25mm have been manufactured and exposed in four different environments. All specimens are designed with a 3/2 lay-up, i.e. two glass fiber prepregs are sandwiched between three aluminum layers. Fig. 37 shows a single prepreg which is exposed from four edges: the problem is two-dimensional. But if the length l equals four times the width b or more, the cross section at l/2 is not influenced by the diffusion in direction y any more. Then, the problem is one-dimensional (diffusion direction z) at cross section l/2, which simplifies further calculations. It turned out, that the 100mm x 25mm specimen is preferable compared with the other one.

The weight gains for the prepregs exposed in different climates are shown in Fig. 38. Straight lines for the prepreg weight gain could be obtained, when plotted in function of square root time. The maximum prepreg moisture content in relation to the relative humidity of the environment was determined by experiments (Fig. 39) and the diffusion coefficients have been calculated. Finally the diffusion rates in GLARE3 could be related to the environmental temperature (Fig. 40). If the diffusion rates are plotted in a logarithmic scale above the reciprocal temperature, they should yield a straight line.

The qualified prepreg in GLARE® behaves according to available physical laws and reliable predictions of moisture concentrations are possible. The basic knowledge for the continuation of the systematic program (items 3) to 7)) is therefore provided.

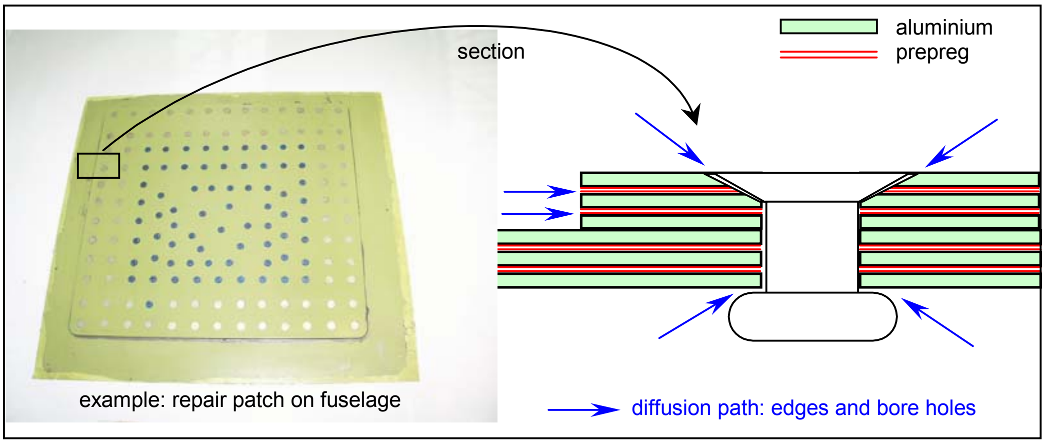

Fig. 36: The moisture penetration in GLARE is limited to the sheet edges and to the bore holes.

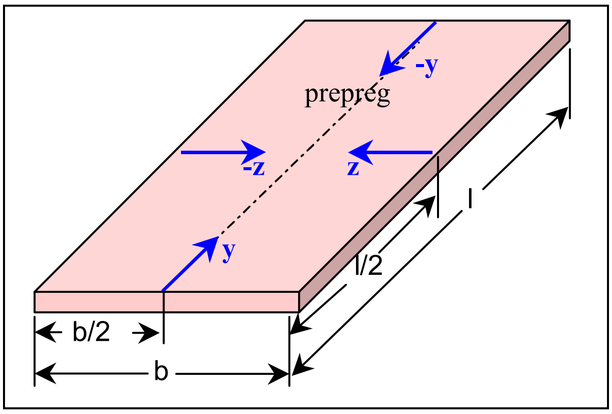

Fig. 37: Two dimensional problem of a GLARE prepreg sample exposed to moisture at the edges.

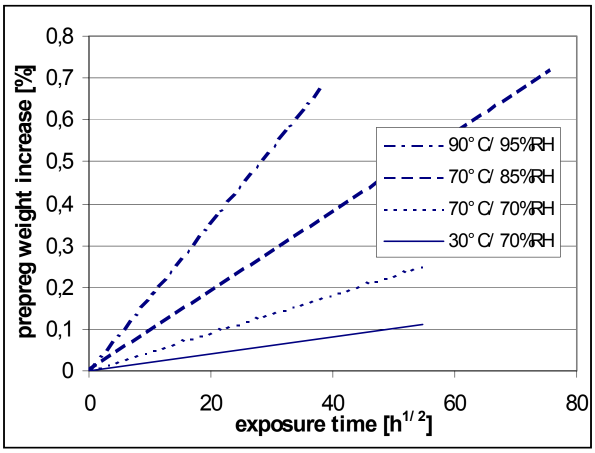

Fig. 38: Weight gain of GLARE prepregs exposed to different environments.

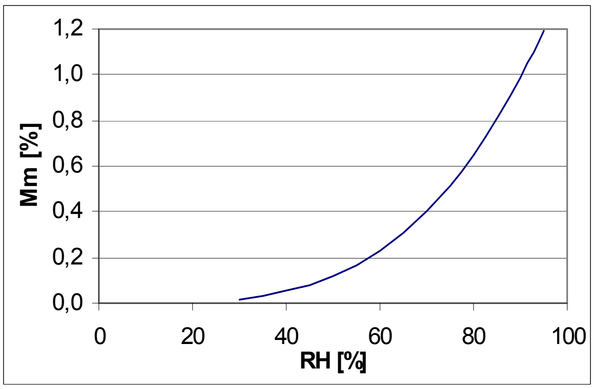

Fig. 39: Maximum prepreg moisture content in relation to the relative humidity of the environment.

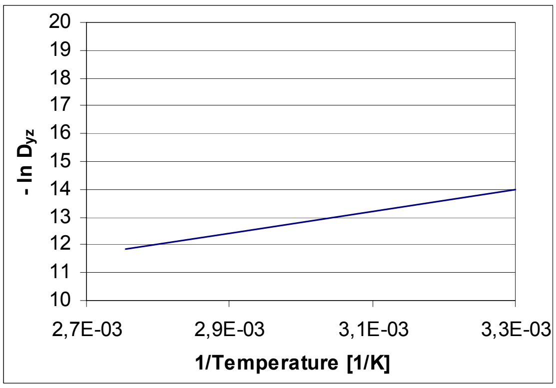

Fig. 40: Calculated diffusion coefficients in GLARE prepregs.

6.3 Fatigue Behaviour of Impact Damaged Composite Aircraft Substructures

Jens Baaran, Michael Gädke, Hans-Christian Goetting and Raimund Rolfes (DLR-SM)

An important aspect for composite aeronautic structures is their damage tolerance behaviour. Low-velocity impact, e.g. tool drop, may induce internal damage, which may not be visible to the naked eye (non or barely visible impact damage, NVID / BVID). For the certification of composite aircraft structures proof is required that undetected internal damage does not grow.

By applying dry preforms (e.g. the so-called non-crimp-fabrics, NCFs) in the manufacturing process, a through-thickness stitching becomes possible, since the fibre material is not pre-impregnated with resin as in the commonly used prepreg materials, Fig. 41. This reinforcement in z-direction is intended to reduce the threat of internal delaminations during impact as well as delamination growth during fatigue loading of pre-damaged structures. However, an enhanced damage tolerance behaviour is traded off for reduced in-plane properties due to an increased ondulation of the fibre material. Nevertheless a possible application of this technology is to improve the bonding by positive locking between skin laminate and stiffener in typical stringer-stiffened aircraft structures.

To permit a comparison of the damage tolerance behaviour of structures made from NCF to structures made of standard prepreg material, predamaged stringer-stiffened panels were subjected to fatigue loading. The NCF-panels and the prepreg-panels were manufactured with the same ratio of fibre orientations in 0°, ±45° and 90° direction. While the fibre-material was the same for both material systems, the resin for the NCF-panels differs from the one used for the prepreg-panels for manufacturing reasons. In two of the NCF panels the stiffener foot was stitched to the skin laminate using a carbon yarn, Fig. 42.

The predamaged panels were subjected to tension-compression fatigue with $R = \sigma_{min} / \sigma_{max} = -1$ at a load frequency of 5 Hz up to 10^6 load cycles.

The results from the testing campaign show that the prepreg-panels exhibited better fatigue behaviour compared to the NCF panels. While none of the prepreg-panels collapsed during the fatigue loading, this was the case for two of the NCF-panels. In one of these the stiffener foot was stitched to the skin laminate. The reason for the inferior fatigue behaviour of the NCF panels may be the comparably brittle resin used for their fabrication. An improvement of the resin system is likely to improve the durability of pre-damaged CFRP structrues made from NCF.

Even large delaminations in prepreg-panels, resulting from 20 Joule impacts near the stringer, permit a fatigue loading close to the static failure load. These delaminations did not grow during the fatigue loading. Delamination growth was

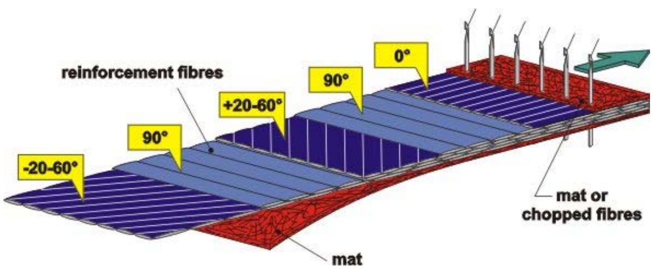

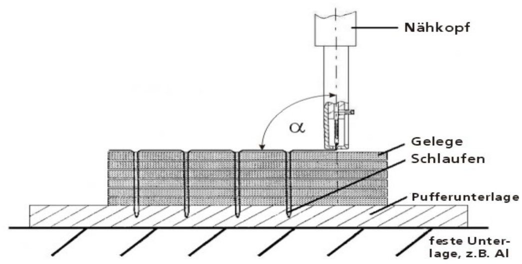

Fig. 41: Left picture: Manufacturing of the so-called NCFs (non-crimp fabrics). Several layers of fibre material are stitched together using a non-load-bearing polyester yarn. Right picture: Structural stitching of dry preforms (e.g. NCFs) with a load bearing yarn, e.g. glass or carbon fibres.

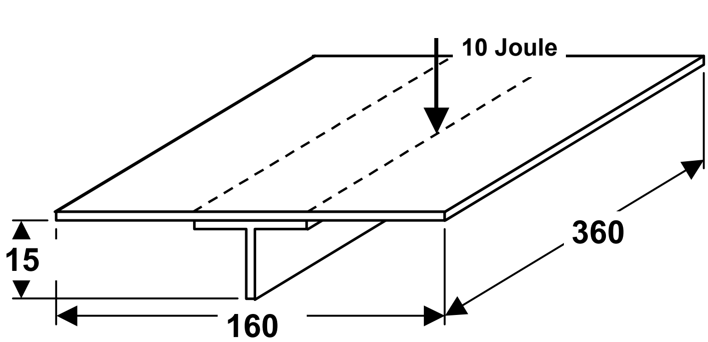

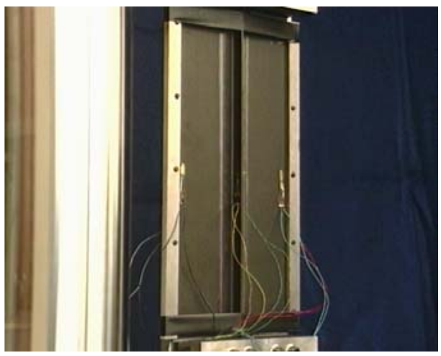

Fig. 42: Left picture: Geometry of the 1-stringer panels with location of the low-energy impact. Right picture: Instrumented panel in the servohydraulic testing rig ready for fatigue loading. The edges of the panels are supported by aluminium bars as anti-buckling guides.

observed for one prepreg-panel where two 10 Joule impacts were introduced in the bay region of the panel.

Due to the limited amount of specimens for the testing campaign and due to the relatively new NCF manufacturing technology a concluding judgement regarding the damage tolerance and durability of NCF structures is not yet possible. Further investigations in this area will be conducted in the frame of the EU FP 5 project FALCOM (Failure, Performance and Processing Prediction for Enhanced Design with Non-Crimp-Fabric Composites). Here the influence of manufacturing parameters of NCF structures on their mechanical performance including fatigue behaviour and damage tolerance will be studied. The presented work was part of the national project „Black Fuselage“, which was funded by the Helmholtz Society. The „Black Fuselage“ project provided accelerated design processes and enhanced structural concepts for better exploiting the specific potential of composite structural design.

6.4 Fatigue of Pultruded Carbon-Fibre Reinforced Composites

O. Krause (DLR-BK) and J. Lowe (Tenax Fibers GmbH)

Pultruded profiles offer a great potential to engineering applications due to their reliable reproducibility and accurate fiber orientation. Using Tenax UTS 5631 12K high strength carbon fibres and an unidirectional fiber orientation, components with a high fibre content and strength are obtained. With the use of the correct material, the fatigue properties thereby can be optimised resulting in a high fatigue strength.

A study was undertaken to investigate the fatigue behavior of unidirectional pultruded profiles using a standard mass production material. Simple coupons were tested under force control in tension at two different R-ratios (R=0.3, R=0.5) and four particular stress levels with a testing frequency of 5 Hz.

The test results at particular stress levels show an underlying scatter, a phenomena often observed for specimens having high stiffness and fiber content, Fig. 43. Apart from the establishment of the S-N-curves the macroscopic investigation of fatigue behaviour was a major objective of the study. Similar to the common experience, the load introduction of the specimens could be identified as the most critical point. Several materials and methods for end-tab manufacture were evaluated, until an optimised solution was achieved. Fatigue damage was initiated at the end of the tabs as a consequence of high shear stress at the tab line and high clamping forces causing high surface pressure. First damage was identified by separation of fibers at the free edge of the specimen beginning at the tab line. During fatigue loading, the number of loose fibers increased rapidly without any significant consequence on the fatigue behavior, Fig. 44.

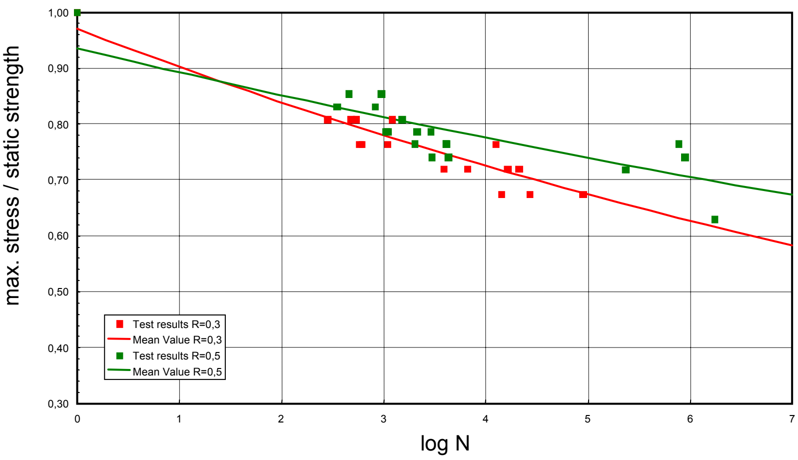

Fig. 43: Fatigue test results of pultruded CFRP.

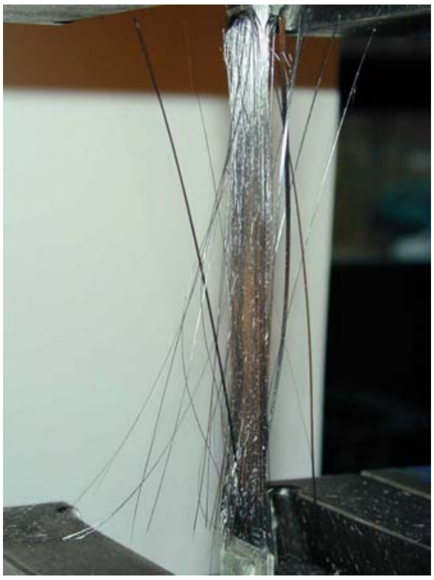

Fig. 44: Pultruded specimen after a number of load cycles corresponding to approximately 20% of lifetime

6.5 Mechanical and Thermographic Characterisation of the Degradation of Angle-Ply FRPs with Respect to the Strain Rate

J. Petermann, O. Mohr, A. Gagel and K. Schulte (TU-HH)

The mechanical degradation of fibre reinforced polymers (FRPs) is characterised by the initiation and progression of multiple failures of different modes such as matrix cracks, interfacial debonding, fibre breaks, and delamination between adjacent plies. The types of failure occurring, the distribution, the onset of initiation as a result of the actual load level and strain rate, and the possible interactions are dependent on test, structural, processing, and environmental parameters.

If fatigue data are normalised by the static strength, the resultant smooth line through the monotonic and fatigue strength frequently displays a knee and an unexpected region of near zero slope at low cyclic lives. This effect may be due to ignoring the difference in strain rate for the two test conditions [16].

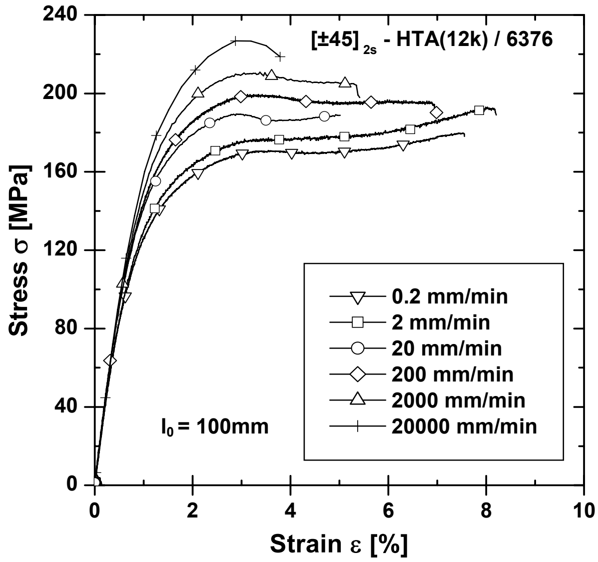

Fig. 45: Effect of quasi-static crosshead velocity on the σ–ε behaviour.

An experimental programme was conducted on $[\pm 45]_{2S}$ HTA carbon / 6376 epoxide specimens with a gauge of $l_0 = 100mm$ and $V_f = 60\%$ to investigate the effects of strain rate on strength and crack evolution under static and fatigue loading conditions. To characterise the (technical) strain rate which is the ratio of the sample's elongation velocity to its initial length, the cross-head velocity (CHV) in units of [*mm/min*] is used.

The dissipated heat of localised damage events and/or distributed material disruption is conducted to the surface. Light microscopy and thermography were applied to record damage events, the latter method by thermal mapping over the surface of the specimen.

Fig. 45 shows that an increase of CHV causes a stiffening and strengthening of the material, i.d. for the yield strength with $R^2 = 0.99$:

$$\sigma_y = 174\, MPa + 10.9\, MPa\, \lg(v\ [mm/min]) \tag{7.1}$$

Formerly conducted sinusoidal stress controlled fatigue tests at $R = 0.1$ and $10Hz$ led to the linear S-N curve with $R^2 = 0.97$ [17]:

$$\sigma_{max}(N) = 210\, MPa - 17.5\, \lg(N) \tag{7.2}$$

Low cyclic lives correspond to maximum cyclic CHVs of about 2000 mm/min. Applying this value to Eq. (7.1) results in $210MPa$, the same stress value as obtained from Eq. (7.2) for $N = 1$.

This shows that the mismatch between strength values determined from tensile tests (according to ISO527 etc.) and extrapolated static strength values from the S-N curve (for N = 1) is a result of strain rates, that are distinctively different in their magnitude. Therefore, if fatigue data shall be normalised with static strength data, the strain rate of the latter has to be chosen appropriately.

Fig. 46 a) shows a thermographic picture series of a specimen surface during a tensile test with CHV = 2000mm/min. Once the yield strain of about 3% is reached, a distinctive temperature pattern forms which corresponds to the fibre orientations. Even close to failure, no extensive fibre rotations are observed. With micrographs from the edges, it could be shown that the temperature pattern is related to the initiation of cracks. Similar strain values for the onset of cracking and the fibre orientation changes were reported in reference [18].

Fig. 46 b) depicts that no temperature pattern could be observed during fatigue testing at $\sigma_{max} = 120$MPa, R = 0.1, and f = 10Hz. The temperature is smoothly distributed over the surface of the sample which indicates a more distributed material disruption. The notable temperature rise above n/N = 0.75 corresponds to the entrance into the third and final stage in fatigue [19]. The nonexistence of a distinctive temperature pattern is supported by x-ray observations showing that no edge cracks or delamination were found outside of the immediate neighborhood of the final failure location.

With respect to the conducted cross-head velocity controlled tests of the investigated material, the following conclusions can be drawn:

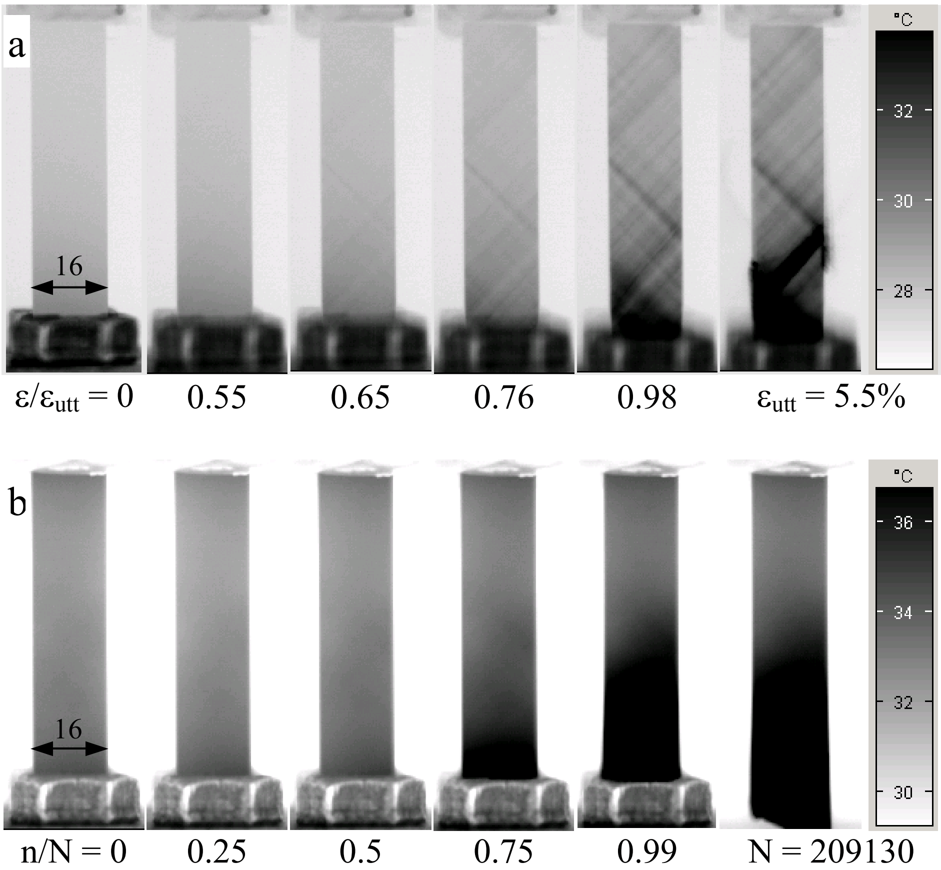

Fig. 46: Thermographic picture series of a specimen surface during a tensile test with CHV = 2000mm/m a) and during fatigue testing at σ_{max} = 120MPa, R = 0.1 b).

- Normalising S-N data with strain rate corrected tensile tests allows to extrapolate the fatigue strength to low cyclic lives and thus to avoid the frequently displayed knee of the S-N curve.
- By using thermography, the damage evolution can be mapped for tensile tests as well as for cyclic tests.
- In static tension, localised damage events, presumably cracks, initiate once the yield strain is reached. In tension-tension fatigue, the material degrades by distributed internal disruption rather than by extensive cracking.

7 FATIGUE AND FRACTURE OF ENGINE MATERIALS AND STRUCTURES

7.1 Lifetime Assessment of Ceramic Thermal Barrier Coatings for Gas Turbine Blades using Fracture Mechanical Damage Parameter

Marion Bartsch, Bernd Baufeld, Klaus Mull and Christian Sick, DLR-WF

Ceramic thermal barrier coatings (TBC) with low thermal conductivity on internally cooled metallic turbine blades give a potential for increasing the gas inlet temperatures in a range of 50-150°C. Since, at higher gas inlet temperatures the remaining lifetime of the blade after failure of the TBC can be extremely short, reliable and practical lifetime assessment for TBCs is required.

Lifetime assessment for TBC systems in service requires realistic testing in order to attain the same damage mechanisms that occur in service. However, realistic tests result in realistic times to failure. That means in the case of TBC systems for aircraft engines about 5,000 to 20,000 hours or 3,000 to 10,000 flights. Accelerating the time dependent damage mechanisms by increasing the test temperature is limited since the damage mechanisms can change with temperature. One approach to overcome this dilemma is to test under most realistic loading conditions, observe simultaneously the damage accumulation, and assess the lifetime from the damage evolution.

One important failure mode of TBC systems is spallation due to delamination cracks near the interface between the ceramic topcoat and the metallic bond coat [20, 21]. Thus, the adhesion strength in terms of fracture toughness or critical energy release rate is an appropriate damage parameter to observe. Lifetime assessment models using fracture mechanics damage parameters, which are directly related to the adhesion/cohesion of the coating, can be transferred to varying coating systems and different loading conditions [22]. For the lifetime model described in [22], the condition for crack growth has been used:

$$G_{actual} > G_c \tag{8.1}$$

with G_{actual}, the actual energy release rate or driving force for delamination crack growth and G_c, the critical energy release rate or crack resistance. G_{actual} and G_c are functions of the loading history, and the lifetime - in number of service or test load cycles to failure N_f - is exhausted when G_{actual} exceeds G_c. G_{actual} is the superposition of the energy release rate due to external loads, $G_{applied}$, and the energy release rate due to accumulated residual stresses, $G_{residual}$. However, available methods for determining the crack resistance or critical energy release rate do not differentiate between changes of the 'true' G_c and changes of residual stresses. Thus, in fracture mechanics tests the equation (8.1) becomes:

$$G_{applied} > G_c - G_{residual} = G_{c,apparent} \tag{8.2}$$

In the case of a service load-cycle, the equation (8.2) can be used for a lifetime assessment if the evolution of $G_{c,\ apparent}$ and $G_{applied}$ is known for the critical sequence of the load cycle.

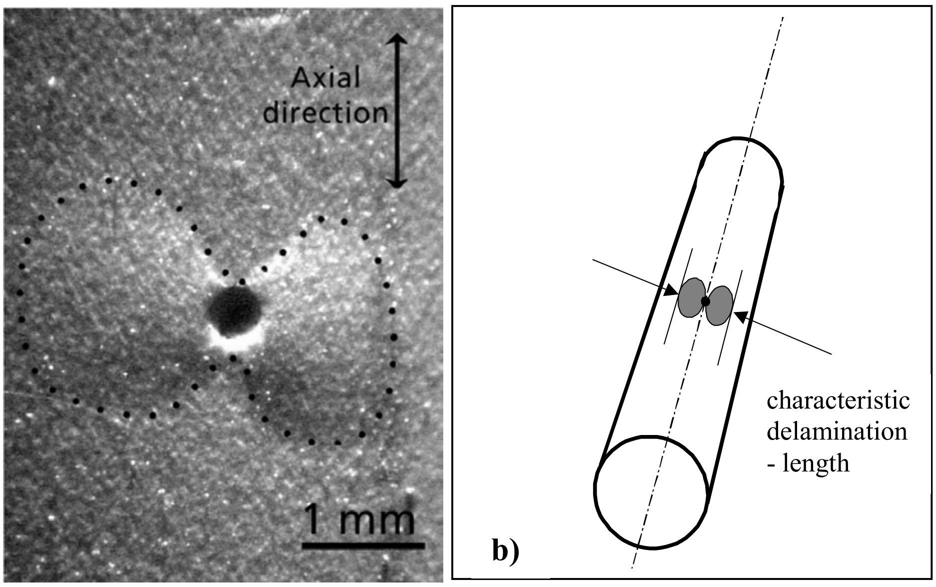

Fig. 47: Butterfly-shaped delamination after Rockwell-indentation, a) optical micrograph of an as coated specimen with 8mm diameter, b) schematic sketch, showing the orientation of the delamination in relation to the cylinder axis (as coated specimen)

Methods for determining the apparent fracture toughness for TBCs are now under investigation. One method which is applicable to curved specimens, which are mainly used in more realistic thermal mechanical fatigue (TMF) and especially in thermal gradient mechanical fatigue testing (TGMF), is the Rockwell indentation test. In this test the surface of a coated cylindrical specimen is indented with a conical Rockwell indenter, using a conventional hardness tester or a displacement controlled universal test machine. The indent results in plastic and elastic deformations of the substrate and the formation of a butterfly-shaped delamination crack close to the interface between metal and the ceramic coating, Fig. 47.

Actually experiments are performed to quantify the changes of the delamination size and geometry as a function of loading history in preceding thermal mechanical tests [23]. Parallel the indentation test will be mechanically analysed in order to calculate the apparent fracture toughness of the TBC system against delamination cracking.

7.2 Oxygen-Induced Intergranular Fracture of Nickel-Base Superalloys - An Example of Dynamic Embrittlement

Ulrich Krupp (USI), William M. Kane, Campbell Laird and Charles J. McMahon Jr (Department of Materials Science and Engineering, University of Pennsylvania, Philadelphia, PA 19104, U.S.A)

Nickel-base superalloys suffer a transition from cycle-dependent transgranular ductile fracture to time-dependent brittle intergranular fracture during fatigue loading, when the service temperature exceeds about 450˚C. As shown by several studies, this transition and the intergranular cracking rate depends strongly on the oxygen supply to the crack tip and the mechanical loading conditions, i.e., static/cyclic, strain rate, hold times and stress intensity at the crack tip. There exist different theories about the mechanism of crack propagation along grain boundaries. They include preferential oxidation of Nb at grain boundaries ahead of the crack tip, injection of vacancies in the grain boundary due to cationic NiO formation or stress-promoted intergranular oxygen diffusion.

The phenomenon of static quasi-brittle intergranular cracking, Fig. 48, has been studied by four-point bending tests on IN718 specimens under fixed displacement at temperatures between 500°C and 650°C and different oxygen partial pressures. Since crack propagation rates reached values of 30µm/s and cracking could be "switched on" within a few seconds by back-filling the evacuated test chamber with air [24], this kind of intergranular fracture seems to be dominated by stress-driven short-range oxygen grain boundary (GB) diffusion followed by decohesion (dynamic embrittlement).

There are several indications that this phenomenon depends strongly on the structure of individual grains, e.g., increasing the fraction of special coincidence site lattice (CSL) grain boundaries by thermomechanical processing (TMP) of the as-received IN718 material (AR) has been found to lead to a higher resistance against intergranular fracture at high temperatures [25]. This is shown in Fig. 49, where stress relaxation of a TMP specimen due to cracking is retarded and slower than for a specimen in the AR condition. To quantify the understanding of the interdependence between dynamic embrittlement and crystallographic misorientation of grain boundaries, bending tests on IN718 bicrystals with different special and random grain boundaries of IN718 were carried out.

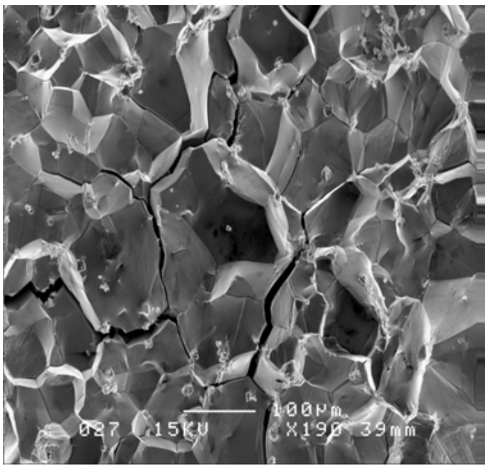

Fig. 48: Intergranular fracture surface of IN718 loaded under fixed-displacement at 650°C in air.

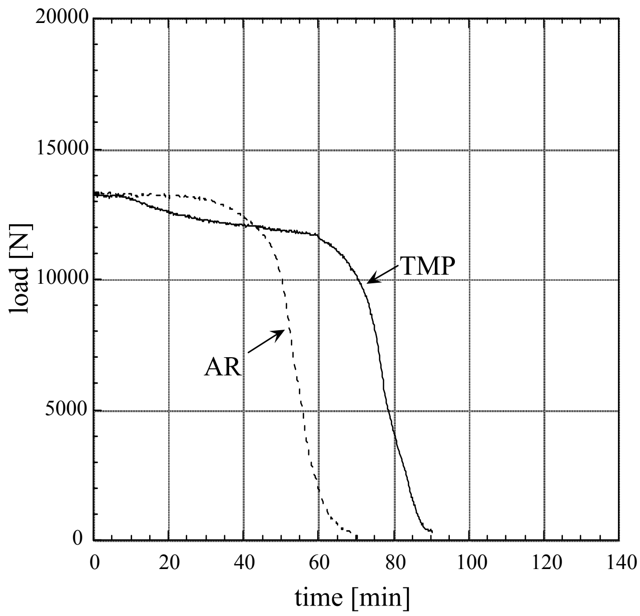

Fig. 49: Load relaxation due to cracking within a TMP (41% CSL grain boundaries) and an AR specimen (20.9% CSL grain boundaries) during four-point bending at 650°C in air

7.3 Thermomechanical Fatigue Behaviour and Life Prediction Methods for Selected High-Temperature Materials

V. Bauer and H.-J. Christ (USI)

Most structural components in high-temperature applications of jet engine, power and chemical plants are subjected to cyclic mechanical and cyclic thermal loading conditions due to start up and shut down processes. Compared with loading conditions at constant temperature, thermomechanical fatigue (TMF) has proven to be more life limiting. In order to extend the operating life of safety relevant components, studies on the damage mechanisms acting under TMF loading conditions and life prediction techniques are crucial. Hence, many research activities in recent years were concentrated particular on the TMF behaviour of materials.

In the present study, thermomechanical fatigue tests are performed on two materials with a different high-temperature behaviour. One is an austenitic stainless steel which is often used for high-temperature structural components, e.g. in Liquid Metal Fast Breeder Reactors (LMFBR) und chemical plants. At high-temperature operating conditions, life of the austenitic steel components is limited due to creep or creep-fatigue damage evolution. In order to evaluate the influence of the operating conditions on the fatigue life, numerous LCF and TMF tests are necessary. The test series with varying temperature range, strain rate and temperature phasing allow to differentiate between single damage mechanisms and to estimate the parameter field where damage mechanisms interact. Based on the knowledge of the parameter field and its effect on the fracture mode, life prediction methods were selected and applied. Beside others the Linear Accumulation of Creep (AC), an energy based approach (FMDF) and the fracture mechanics based D_{CF}-method were deployed. The consideration of the damage mechanisms for life calculation shows that the prediction is accurate if one mechanism dominates. Moreover, none of the techniques is capable to predict fatigue life satisfactorily for the entire parameter spectrum so that continuos improvement in life prediction techniques remains in focus of the study.

The second material is a γ-TiAl based intermetallic alloy with promising properties for jet and automotive engines. It has received considerable attention because of its high specific strength and stiffness, good oxidation resistance at high-temperature, and better creep resistance as compared to conventional titanium alloys. However, its low ductility and toughness restrict its applications. Furthermore, first investigations on high-temperature fatigue behaviour in different surroundings showed that the environmental degradation is responsible for a premature rupture. The mechanism for this is well established: oxygen (and nitrogen) diffuse into titanium and form a brittle subsurface layer. During cycling this layer can crack, and if the fatigue crack growth threshold is exceeded, these surface cracks propagate, leading to a reduced fatigue life as compared with unexposed material. The aim of the project is to quantify the relevant damage mechanism during the LCF and TMF tests (particular the environmental contribution depending on temperature phasing) and to establish the life prediction methodology based on linear damage accumulation. At this time, the cyclic ΔJ-approach extended by an oxidation parameter promises reasonable prediction results.

Of particular interest for the most life prediction methods is the information about the cyclic stress-strain response of the material. For this reason a modified multi-component model for the calculation of Cyclic Stress-Strain curves (CSS) is used. The model can be applied for a variety of materials. It is able to consider the strain-rate dependency as well as creep effects at high-temperatures in case of austenitic stainless steels and thus provide reliable input data for life pre-

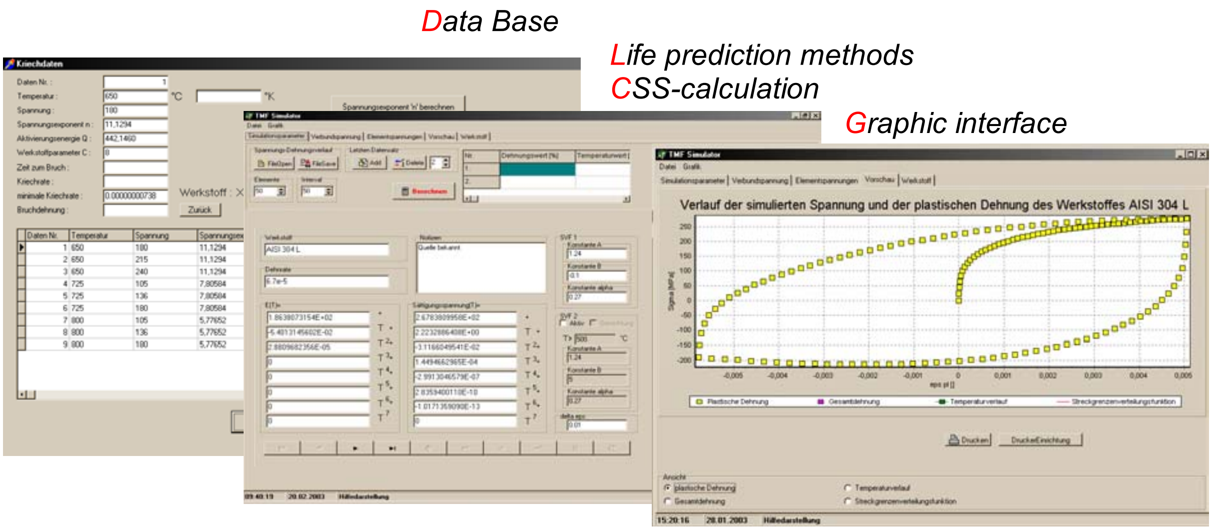

Fig. 50: Schematic design of the computer program for materials data storage and fatigue life prediction methods with graphical interface.

diction methods. The large amount of input data and test parameters are stored in a data base which is linked with the program for calculating CSS response.

This computer tool which also contains the applied life prediction methods is a concomitant development of the project. In Fig. 50 the schematic design of this computer program is demonstrated. The underlying data base stores all materials data and data derived from the experiment. An implemented graph interface enables simple plots e.g. hysteresis loops or Norton plots of this data. The program is used for a documentation of all data evaluation methods and prediction techniques used in the framework of the project. It is written in such way that external users can easily adapt it to their particular needs.

7.4 Thermohydrogen Processing (THP) of Metastable Beta Titanium Alloys

G.M. Lohse and H.-J. Christ (USI)

Beta titanium alloys have an ongoing and developing role in the aeronautical, aerospace and recently consumer industry due to of their attractive strength-to-density ratio, excellent corrosion resistance, deep hardening heat treatment potential and inherent ductility as a result of the body centered cubic (bcc) structure of the high temperature beta phase of titanium.

Generally, hydrogen is known to deteriorate the mechanical properties and lead to brittle fracture behaviour of most structural alloys. Hydrogen uptake mainly takes place during production, surface treatment and in service under respective environmental conditions. As opposed to the embrittling effect of hydrogen, a positive effect on the mechanical properties of titanium alloys may result under certain conditions. This is due to the fact that hydrogen stabilizes the beta phase of titanium and can therefore be used to optimize the microstructure by means of thermohydrogen processing (THP).

The object of this ongoing study is to investigate the effect of hydrogen on the microstructure and to characterize the variation of the mechanical properties in metastable ß titanium alloys by means of thermohydrogen processing. Especially in the investigated metastable ß-titanium alloys hydrogen has strong influence on the microstructure and this provides the possibility to optimise final mechanical properties.

The present study deals with two commercial titanium alloys used in TH processing. ß-titanium alloys Timetal®LCB (low cost beta, Ti-6.8Mo-4.5Fe-1.5Al) and Timetal®10V-2Fe-3Al were hydrogenised by means of hydrogen charging from helium/hydrogen gas mixtures during heat treatment with variable hydrogen concentration. Concentrations were reproducibly established following Sieverts' law. Fig. 51 shows experimentally determined plots of the hydrogen concentration in LCB representing the solubility data, versus the square root of hydrogen partial pressure in the gas phase. It can be seen that for hydrogen the solubility increases with decreasing temperature. Furthermore, the isothermal plot at 830°C indicates that the solubility in the alloy up to a partial pressures of 25 mbar follows strictly the Sieverts' law.

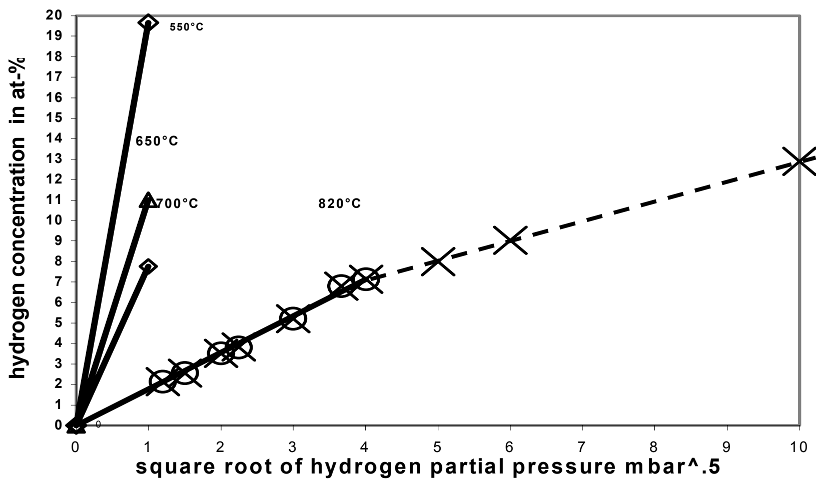

Fig. 51: Linear relationship between hydrogen concentration and the square root of partial pressure for hydrogen charging of LCB at various temperatures.

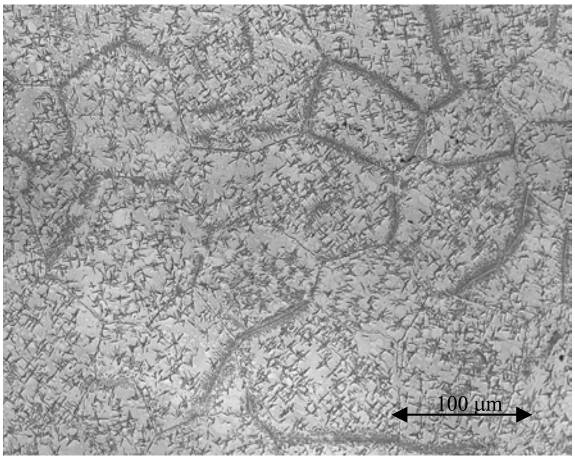

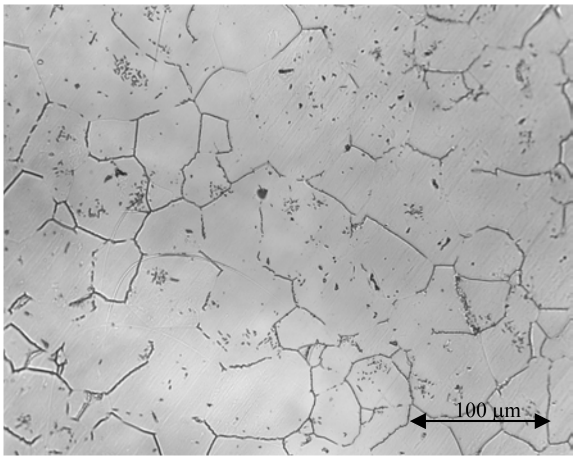

(a) (b)

Fig. 52: Microstructures of LCB after solution annealing and heat treatment at 700°C and 610°C with subsequent water quenching. Hydrogen content in (a) is 3 at-% and in (b) is 12 at-%

Fig. 52 show the microstructure of LCB after solution annealing and heat treatment for 4 hours at 700°C and 610°C, respectively, with subsequent water quenching. The hydrogen content of the material shown in Fig. 52 (a) is 3 at-% and in Fig. 52 (b) 12 at-%. The heat treatment led in both cases to two-phase microstructures consisting of bcc ß-matrix with α-precipitates. The sample of Fig. 52 (a) shows a higher volume fraction of secondary hexagonal α-phase than the sample of Fig. 52 (b), because of the lower hydrogen content. Furthermore, the lower volume fraction of secondary α-phase in Fig. 52 (b) indicates that LCB with a content of 12 at-% of hydrogen has its beta transus very close to 610 °C.

In the future study the result of the hydrogen effects in terms of the solubility and the change of beta transus will be used to develop a three step THP treatment, consisting of hydrogen charging, solution annealing above the beta transus and ageing in combination with hydrogen release. This process provides the opportunity to establish a microstructure with less grain growth during solution annealing and higher volume fraction of the strengthening α-precipitates after ageing as compared to the standard heat treatment. The final goal is to optimize mechanical properties in a way that an improved strength and fatigue limit results.

7.5 Thermomechanical Fatigue Behaviour of a γ-TiAl Sheet Material

P. Schallow and H.-J. Christ (USI)

High specific strength, good creep resistance combined with sufficient oxidation and hot gas corrosion resistance qualify γ-titanium aluminides as new candidate materials for several aero-engine applications. In particular, the production of sheets should open additional new application fields for TiAl alloys. Due to reasonable hot gas corrosion resistance TiAl sheets can be used as gas leading parts in aircraft engines. The work presented resulted from a study carried out in the framework of an European 5th Framework Program named DOLSIG (Development of Lightweight Stiff Static Sheet Structures In Gamma Titanium Aluminide). The objective of this Project is to manufacture an exhaust cone made of γ-TiAl sheet material, Fig. 53. In order to ensure safety and reliability of such components under service conditions, respective testing methods, which account for the complex thermal and mechanical loading conditions of the components in service need to be applied. Therefore, within this study main emphasis was put on the characterization of the thermomechanical fatigue behaviour and its influence on the evolution of the microstructure. To elaborate the characteristics of thermomechanical fatigue, the differences in the deformation behaviour as compared to isothermal tests carried out under similar conditions are pointed out.

Fig. 53: Exhaust cone.

The sheet-material investigated in this study has a thickness of 1 and 1.5 mm, respectively, and was produced via an ingot route by PLANSEE AG. All tests were carried out on specimens in the as-received condition. This so-called "primary annealed" condition of the material has a microstructure comparable to that of "near-γ" consisting of equiaxed globular γ–grains and small α_2-grains at grain boundaries and triple points. The well-known brittle-to-ductile transition (BDT) of this class of alloys lies at about 650 °C and is characterized by a pronounced increase in the monotonic fracture strain with increasing temperature. Regarding fatigue and fracture behaviour, the BDT is of particular interest for the TMF tests which were carried out in in-phase (IP) and out-of-phase (OP) mode. During testing three temperature intervals were taken, a first one which fully incorporates the BDT, a second one where the thermal cycle lies predominantly below BDT and a third one which is above the BDT. Tests were carried out in total (mechanical) strain control with a triangular command signal. To account for the effect of imposed mean stresses on the fatigue behaviour the alloy was tested at R-values of 0.1 and – 1. For this purpose, it was necessary to design and optimize an Anti-Buckling Device, which allows for testing under compressive stresses. Moreover, two strain ranges of $\Delta\varepsilon = 0.6$ and 0.7 % were applied.

In-phase testing under symmetrical push-pull conditions results in fatigue life which is comparable to that of isothermal tests at maximum temperature. Generally, IP testing leads to an increasingly negative mean stress. This increase in mean stress is particularly pronounced during the first 100-200 cycles, Fig. 54. Moreover, IP testing leads to cyclic softening manifesting itself in a drop of the stress amplitude of up to 20 %. OP testing was found to be most detrimental. In this case fatigue life is affected by the resulting positive mean stress leading to a fatigue life which is well below that obtained in isothermal tests carried out in the temperature range considered.

SEM studies on the fracture surfaces revealed a more transgranular cleavage type of fracture with cracked large γ-grains below BDT. On contrast, at increased temperatures, in particular above BDT, a more dimple type of fracture could be observed. TEM studies on OP tested specimens revealed a bundle-like dislocation arrangement and indicate the occurrence of multiplication processes (prismatic dislocation loops). It was found that mechanical twinning contributes to the deformation process in IP as well as in OP testing. Beyond this, small dislocation-free γ-grains were found in IP tested specimens only indicating the onset of dynamic recrystallization under these test conditions, Fig. 55.

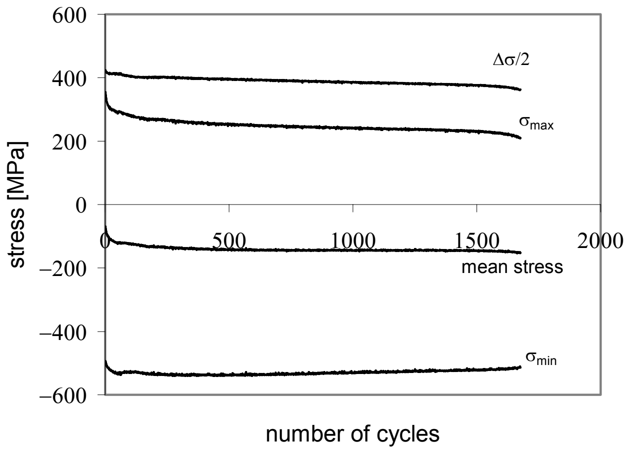

Fig. 54: Cyclic softening and evolution of mean stress during an IP test (500-750 °C, R=-1, $\Delta\varepsilon$=0.7 %).

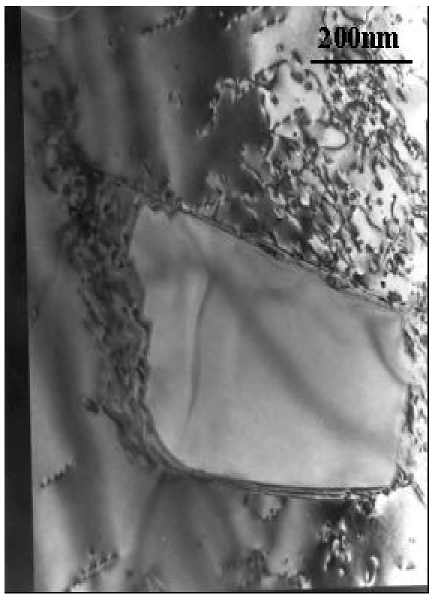

Fig. 55: Dislocation-free recrystallized γ-grain (onset of dynamic recrystallization during an IP test)

8 STRUCTURAL HEALTH MONITORING AND NON-DESTRUCTIVE TESTING

8.1 Benefits from Application of Structural Health Monitoring (SHM) Systems to Civil Transport Aircraft

Jens Telgkamp (Airbus-D)

The design and dimensioning of aircraft structure has to fulfil several requirements according to the airworthiness regulations. Up to now, it is not common to consider the use of Structural Health Monitoring (SHM) systems in large civil transport aircraft.

In future, the consideration of SHM systems will result in several benefits to the aircraft manufacturers and aircraft operators. These benefits can be grouped in benefits which will be available in near future (short-term benefits) on the one hand, and benefits which will be available after some more years of development time (long-term benefits) on the other hand.

Today it is assumed that short-term benefits will mainly result from monitoring of known hot-spot areas of the aircraft type under consideration. By this SHM application, time-consuming and expensive non-scheduled inspections can be avoided. Furthermore, short-term benefits may also result from monitoring of known cracks in the aircraft structure.

However, an emphasis is also put on long-term benefits. These benefits will in future result from consideration of the SHM system already during the aircraft design phase. With this philosophy, the damage tolerance concepts based on crack growth and residual strength (metallic structures) or the compression after impact criteria (composite structures) can be applied in a different way, compared to a structure design without SHM systems. The criteria mentioned will then be less important to the dimensioning of the structure, compared to today’s design philosophy. Therefore, the

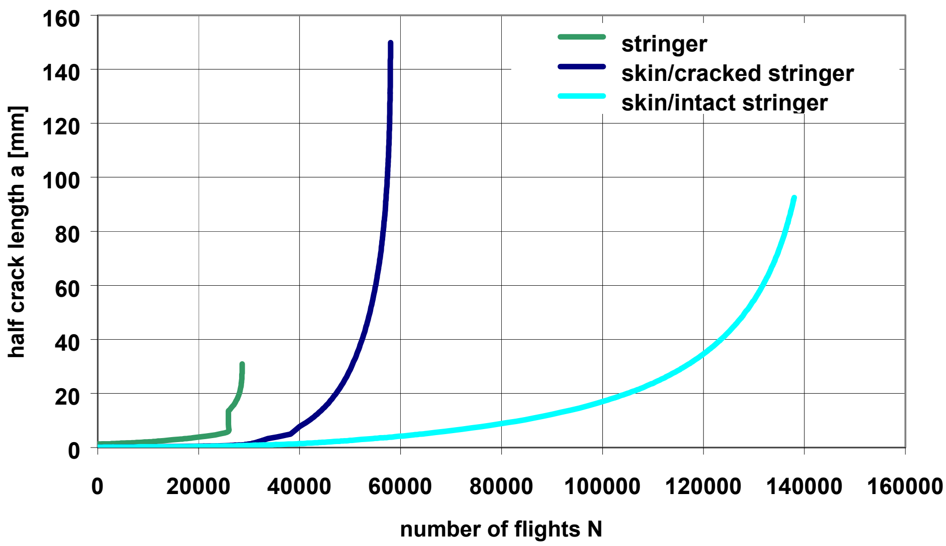

Fig. 56: Crack growth in a panel over cracked stiffener and over an intact stiffener.

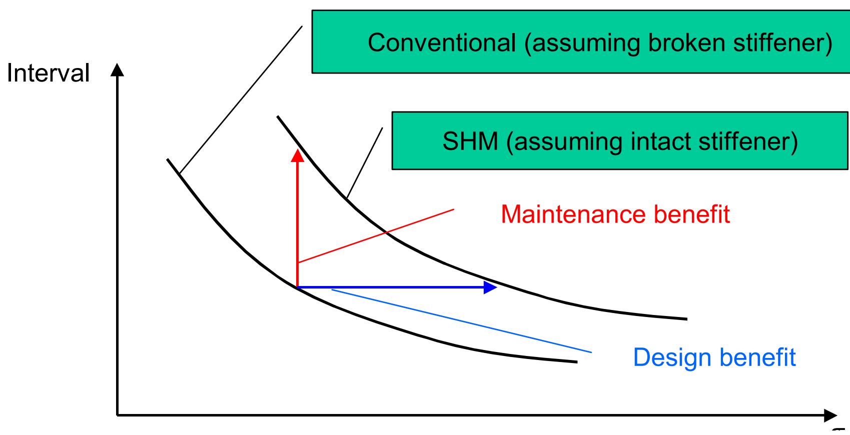

Fig. 57: Design benefit and maintenance benefit from consideration of SHM systems in the design phase of new aircraft.

design will be optimized, offering the possibility to save weight on metal and composite structures while maintaining airworthiness and fulfilling current and future regulations.

The possibility of saving weight by consideration of SHM in the aircraft design phase is explained using the following example of application to a metal structure: It is assumed that an SHM system is used to monitor internal stiffeners (here: stringers). According to the state-of-the-art, these members are not monitored and cracks can not be detected in scheduled maintenance. Therefore, it has to be assumed in crack-growth calculations that the stringers are broken. With the use of the SHM system for monitoring the stiffeners, the crack growth calculation may be performed assuming an intact stiffener. Therefore, the dimensioning of the panel will lead to a significantly different result, as the calculated crack propagation curves in Fig. 56 indicate. Panels sized by crack growth and residual strength criteria can be dimensioned with a different philosophy if the SHM system is considered during the aircraft design phase.

The benefit from this re-dimensioning can be used in different ways, see Fig. 57:

- The **Maintenance benefit** leads to longer inspection intervals and/or threshold while keeping the panel thickness and therefore the stress level in the panel unchanged.
- The **Design benefit** leads to a different dimensioning (thinner panel and therefore higher stress level) while keeping the inspection schedule constant.

Since the maintenance schedule of civil transport aircraft is a complex issue and is more or less fixed due to other components, the Design benefit is of main interest, leading to a **weight saving**, compared to today's dimensioning philosophy.

In the example presented above, the dimensioning of a metallic panel sized by damage tolerance criteria is investigated. However, benefits should also be possible for composite structures. For example, the "Compression after Impact" criterion, which is limiting the compression allowables for composite materials, may be challenged in future with the consideration of SHM systems in composite design, leading to a less conservative dimensioning while maintaining the high airworthiness standard.

The research will be continued for metallic components as well as for composite components.

8.2 Integration of Vibration Monitoring Functionality into an Aircraft Engine Control Unit

Ch. Pritzkow and R. Rennert (IMA)

In trying to operate aircraft engines more economically and safely the idea came up to integrate a vibration monitoring system into an aircraft engine control unit. For this purpose an existing and well proofed system for vibro-acoustic diagnostics was adapted to the survey of an aircraft engine. The manufacturer of the aircraft engine control unit is Diehl Avionik Systems Ltd., Überlingen, one of the project partners.

An existing engine control unit was equipped with a special data logging unit capable of vibration measurements. Concepts for dynamic and permanent data storage were created, implemented and field-tested. Effective methods for signal

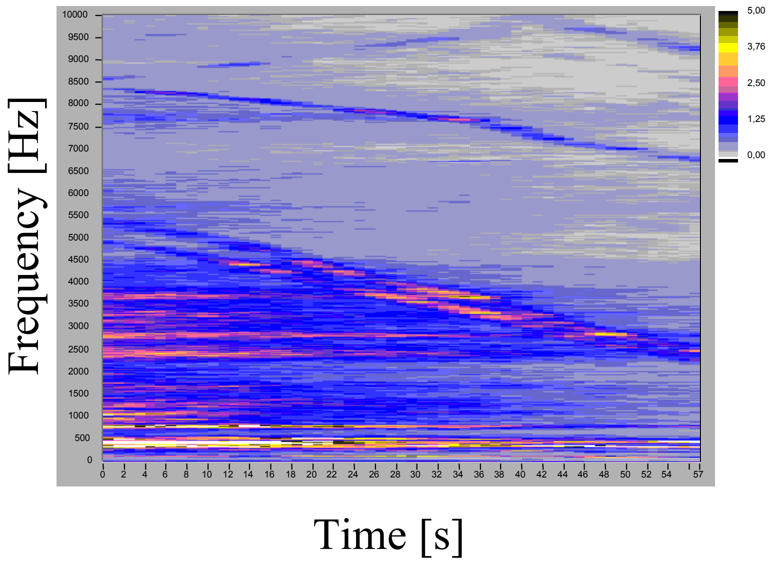

Fig. 58: Intensity plot of engine acceleration spectra during a shut down
(yellow = high acceleration, blue to grey low acceleration)

analysis were used like power spectra and envelope spectra.

In Fig. 58 the intensity plot of an acceleration power spectra in an aircraft engine during shut down is shown. It marks the possibility to find significant vibration patterns in the aircraft engine noise.

After measuring accelerations, logging them and calculating some kinds of frequency spectra the estimation of characteristic vibration values of a certain aircraft engine will be possible. Therefore a condition monitoring for more efficient maintenance of aircraft engines can be carried out. Additionally a new algorithm for online unbalance estimation was developed. It accomplishes unbalance monitoring during high dynamic speed changes. The vibration monitoring system was integrated into an aircraft engine control unit. To do this, some concepts for memory reduction had to be implemented. The trial on real aircraft engines in a test stand was successful.

This project was funded by the Federal Ministry of Education and Research.

8.3 Proposal: Usage Related Availability and Safety of Structural Systems

A. Büter (LBF)

The economic efficiency and competitiveness of an environment-friendly transportation system depends on safety, availability and maintenance of single highly loaded structure components. Up to now these components have been changed in fixed maintenance intervals irrespective of any usage related conditions. With the knowledge and evaluation of the component conditions, life cycle costs can be reduced by means of an optimised maintenance and fit for purpose design.

Service life and endurance strength are mainly determined by the following parameters:

- Random operational loading combined with special loading events and long term use
- Design
- Influence of materials and the manufacturing process
- Environmental conditions
- Quality assurance and monitoring

The interaction of the assembly made up of several parts e.g. like gears, the use of different materials (steel, cast iron, light metals, composites) and overlapping random loading during long term use, results in complex stresses and damage mechanisms:

- Material fatigue under random, multiaxial loads with highly dynamic load peaks, thermo-mechanical loading and aggressive environmental stresses, etc.
- Fretting corrosion in the area of the shrink fit.
- Damage to treads by rolling contact due to abrasion, wear and cyclic, plastic deformation in the surface zone
- Bearing damage due to fatigue, grease deterioration, local plastic deformation.

Such damage may lead to considerable danger and a reduction of safety as well as to a loss of comfort and a decreased performance, if not avoided or recognised in time. At least it will lead to an impairment of availability and an increase in maintenance expenditure.

The state of the art is:

- No safe method for crack evaluation in advance is available to assess the risk potential;
- Furthermore, there are no suitable methods for on-line detection and monitoring;
- An off-line ultrasonic-diagnosis for crack detection is in use,
- The possibility of a three-dimensional acceleration measurement to detect anything conspicuous is feasible in principle, but its assignment to the existing cause must be examined.

If the design is expected to demonstrate an increased performance, non-destructive testing must be closely combined with service life and fatigue concepts and their evaluation methods (as for example in damage-tolerance-concepts) and even with the permanent monitoring (health monitoring) of all areas of structure components identified to be safety relevant.

Based on extensive experimental and numerical research, the objective is the realisation of such a usage dependent monitoring system to a stage where it can be implemented in highly loaded structure components, to guarantee safety and optimise availability, maintenance and life cycle costs. In order to realise this, an efficient management system of operational loading data and its transformation into useable knowledge about the condition of structure components as well as a better understanding of usage dependent damage mechanisms, expansion and interaction with the structure are needed. Based on this knowledge, *new transport-specific advanced design and production techniques, leading to improved quality, safety, and cost-effectiveness of environmentally friendly vehicles* can be achieved.

The highly loaded and safety relevant structure components must be classified by operational conditions and evaluated by the safety relevance. The fundamental influences of design, materials and the manufacturing process on the durability are independent of the structure component itself. A more basic approach to research on this topic can be used. For the understanding of damage mechanisms, expansion and damage-structure-interaction, the individual operational conditions of the various structure components are important. The development of the monitoring system must take this into account.

The determination and evaluation of defects, incipient fractures and the remaining life and the development of new models for a local (structure component) and a global (railway system) monitoring system based on extensive numerical and experimental research are key parts of the work which have to be done.

8.4 Ultrasonic Testing on Friction Stir Welded Aluminium Alloys

Günter Staniek (DLR-WF), Wolfgang Hillger (DLR-SM) and Claudio Dalle Donne (DLR-WF)

Typical weld defects found in friction stir welds of thin section aluminium alloys were detected and classified by the ultrasonic pulse-echo method [26]. The ultrasonic tests were performed on immersed 4 mm thick butt welds with a high-frequency ultrasonic inspection system. By means of vertical incidence, it was possible to identify almost all the volumetric defect geometries above a critical size. Diagonal incidence is primarily suitable for detecting flaws and unbonded zones in the root region of the weld. Although the exact shape of such unbonded regions cannot be derived from the ultrasonic images, it is possible to determine the exact location and the depth from the time of flight D-scans, Fig. 59.

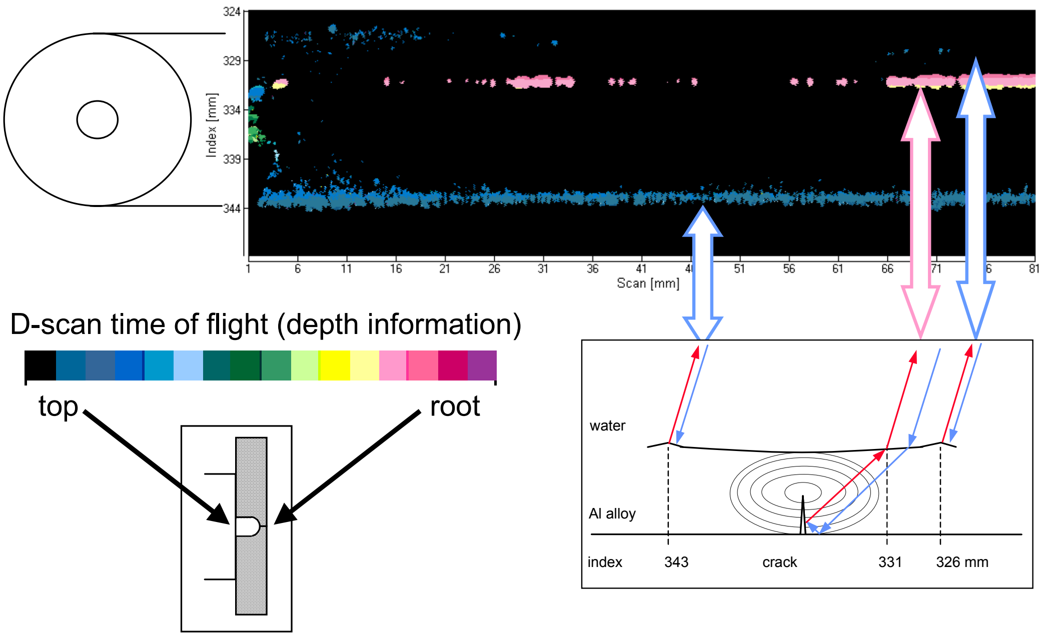

Fig. 59: Root flaw due to incomplete joint penetration during FSW detected with an ultrasonic test method.

9 INVESTIGATIONS OF GENERAL INTEREST

9.1 Fatigue Behaviour of Open-Cell Metal Foams under Isothermal and Thermomechanical Loading Conditions

A. Ohrndorf, U. Krupp and H.-J. Christ (USI)

In the last few years much effort has been placed on the development of numerous processing routes for closed-cell and open-cell metallic foams with the objective to improve the homogeneity of their structure. Now, several foams with outstanding properties are available, which fulfil the needs of industrial applications. The low cost closed-cell aluminium foams have been established as crash energy absorbing materials in technical components such as bumpers of railway trains, cars or nuclear waste containers. The mechanical behaviour of metallic foams in the case of monotonic compression is fairly understood and can be controlled by adjusting the porosity of the foam and the microstructure of the cell wall material. For more advanced structural applications, not only monotonic but also cyclic loading of the foam components has to be taken into account.

Precision cast open-cell foam structures using high-strength cell strut materials such as steel or Ni-base alloys have the potential of being infiltrated with another (light-weight) metal with the effect of reinforcement. One example of a possible application of this infiltration method is the local reinforcement of highly stressed regions in magnesium gear boxes by means of foam inlays to avoid cracking. In addition, components may be exposed to fluctuating temperatures making the knowledge of thermomechanical fatigue behaviour important.

In the present study two open-cell foams with different cell strut materials (AlSi9Cu3 and α-brass) but with identical cell structures were tested both in monotonic loading and in isothermal fatigue. Rectangular foam specimens, which were glued to a special specimen mount were used for the room temperature tests. Low cycle fatigue tests were conducted on a servohydraulic testing machine applying load control with a stress ratio of R=-1.

Cycling of the temperature for thermomechanical fatigue tests was established by an innovative temperature-control system, which was required since the commonly-used induction heating is not applicable with open-cell foam structures. The new temperature chamber is heated by means of a hot air fan and cooled by compressed air as it is depicted in Fig. 60. The temperature is controlled by the flow rate of the cooling air. In order to conduct tests with temperatures exceeding 200°C, both ends of the specimens were cast-infiltrated with a Zn-alloy serving as specimen mounts. Because of the high temperatures during the infiltration, only brass foams were tested at elevated temperatures. This experimental set-up makes thermomechanical fatigue tests in strain control and with temperatures fluctuating from 50°C up to 300°C possible.

Isothermal tests revealed completely different damage mechanisms being active in monotonic compression and monotonic tension of open-cell foams. Whereas in compression damage is related with the formation and the subsequent collapse of deformation bands resulting in an expanded regime of plateau stress, in tension a relatively uniform distribution of strain is observed. Here, the amount of plastic deformation at fracture is strongly influenced by the ductility of the cell strut material and changes from about $\varepsilon = 1\%$ with AlSi9Cu3 to more than $\varepsilon = 20\%$ for brass foam.

The detrimental influence of tensile stresses, particularly

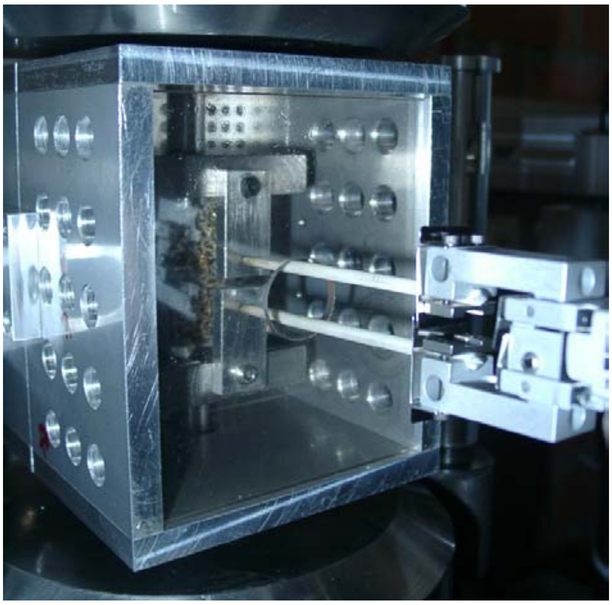

Fig. 60: Temperature chamber for the realisation of TMF tests on open-cell foams.

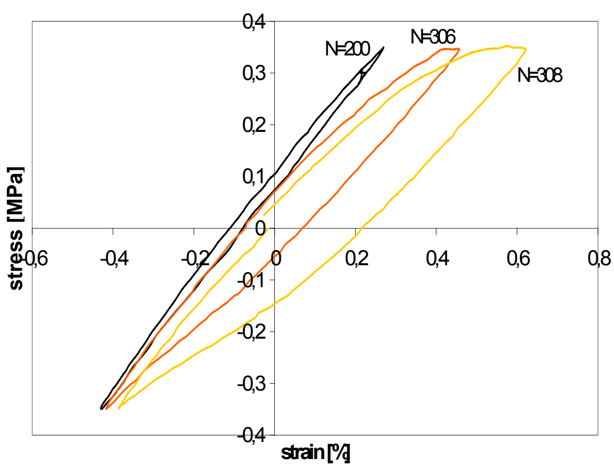

Fig. 61: Hysteresis loops taken from the final stage of a fatigue test of an open-cell aluminium foam.

apparent from the monotonic tests of the brittle aluminium foam, also manifests itself in the fatigue behaviour. Progressive lengthening or shortening of the specimens that can be considered as a kind of cyclic creep was found to occur. During the final stage of the fatigue test, the propagation of a dominant crack leads to an increase of the compliance in the regime of tensile stresses. However, in compression the fractured cell struts get in contact again, and hence, the change of stiffness is not very pronounced in the compressive half-cycle. In Fig. 61 the evolution of the hysteresis loops shows the decreasing stiffness of the specimen caused by the propagating crack. The existence of fatigue striations found by SEM examination of the fractured cell struts reveals that the damage mechanism is a combination of cyclic creep and fatigue crack propagation through the cell struts.

The mechanical behaviour of the foams under thermomechanical loading conditions is compared to that under isothermal fatigue at room temperature and at elevated temperatures and the mechanisms of fatigue damage for each loading condition are examined applying optical and scanning electron microscopy.

10 REFERENCES

[1] Antemia, P.: Full Scale Fatigue Test, Grob Aerospace, Doc. No. :GP-G109B-000001, 2003.

[2] Dalle Donne, C., Lima, E., Wegener, J., A., Pyzalla and Buslaps, T: Investigations on Residual Stresses in Friction Stir Welds, 3rd International Symposium on Friction Stir Welding, Kobe, Japan, 27 and 28 September 2001, TWI, cd-rom.

[3] Dalle Donne, C. and Raimbeaux, G.: Residual Stress Effects on Fatigue Crack Propagation in Friction Stir Welds, 10th International Conference on Fracture, ICF 10, Elsevier Science Publ., 2001, cd-rom.

[4] Juricic, C., Dalle Donne, C. and Dreßler, U.: Effect of Heat Treatments on Mechanical Properties of Friction Stir Welded 6013, 3rd International Symposium on Friction Stir Welding, Kobe, Japan, 27 and 28 September 2001, TWI, cd-rom.

[5] Bär, J. and Volpp, T.: Vollautomatische Experimente zur Ermüdungsrissausbreitung, Materialprüfung, 43, 6, 2001, pp. 242-247.

[6] Bär, J., Rödling, S., Broll, M. and Gudladt, H.-J.: Einfluß von Überlasten auf die Ausbreitung von Ermüdungsrissen in der Aluminiumlegierung 7075 T 7351, Materialwissenschaft und Werkstofftechnik, 22, 2002, pp. 177-183.

[7] Paris, P. C. and Erdogan, F. J.: A Critical Analysis of Crack Propagation Laws, Journal of Basic Engineering, 85, 1960, pp. 528-534.

[8] Klesnil, M. and Lukás, P.: Influence of Strength and Stress History on Growth and Stabilisation of Fatigue Cracks, Engineering Fracture Mechanics, 4, 1972, pp. 77-92.

[9] Erker, A.: Sicherheit und Bruchwahrscheinlichkeit, MAN-Forschungsheft, 8, 1958, pp. 49-62.

[10] Rossow, E.: Eine einfache Rechenschiebernäherung an die dem Normal Scores entsprechenden Prozentpunkte, Zeitschrift für wirtschaftliche Fertigung, 59, 1964, pp. 596-597.

[11] Wheeler, O. E.: Spectrum Loading and Crack Growth, Journal of Basic Engineering, 92, 1972, pp. 181-186.

[12] Remmers, J.J.C. and de Borst, R.: Delamination buckling of fibre metal laminates, Composites Science and Technology, 2001, pp. 2207-2213.

[13] Vlot, A. and Gunnink, J.W.: Fibre Metal Laminates - an Introduction., Kluwer Academic Publishers, 2001.

[14] Hagenbeek, M., Remmers, J. J.C. and de Borst, R.: Implementation of the thermomechanical solid-like shell element in b2000, 4th B2000 Workshop Proceedings. SMR Engineering and Development, October 2002..

[15] Hashagen, F.: Numerical analysis of failure mechanisms in fibre metal laminates, PhD. thesis, Technische Universiteit Delft, 1998.

[16] Sims, G. D. and Gladman, D. G.: Effect of test conditions on the fatigue strength of a glass-fabric laminate: Part A-Frequency, Plastics and Rubber: Materials and Applications,1978, pp. 41-48.

[17] Petermann, J., Hinz, S. and Schulte, K.: A nonlinear damage accumulation model for carbon fibre reinforced angle-ply laminates, Proceedings 10 th European Conference on Composite Materials (ECCM/10), Sol, H. and Degrieck, J. (Ed.),2002, pp. 328:1-7.

[18] Lafarie-Frenot, M. C. and Touchard, F.: Comparative in-plane shear behaviour of long-carbon-fibre composites with thermoset or thermoplastic matrix, Composites Science and Technology, 52, 1994, pp. 417-425.

[19] Quaresimin, M.: Fatigue of woven composite laminates under tensile and compressive loading, Proceedings 10 th European Conference on Composite Materials (ECCM/10), Sol, H. and Degrieck, J. (Ed.),2002, pp. 191:1-8.

[20] Bartsch, M., Mull, K. and Sick, C.: Effects of Thermomechanical Fatigue Loading on Damage Evolution and Lifetime of a Coated Super Alloy, ASTM-STP 1417, Fatigue and Fracture Mechanics: 33rd Volume, ASTM, West Conshohocken, USA, 2002, pp. 147-160.

[21] Baufeld, B. and Bartsch, M.: Thermo-mechanical Fatigue of Thermal Barrier Coating Systems, Proceedings of the 8th International Conference Fatigue'2002,2002, pp. 2493-2500.

[22] Bartsch, M. and Baufeld, B.: Fracture Mechanical Approach for a Lifetime Assessment of Ceramic Thermal Barrier Coatings, Proc. of the European Conference on Fracture - ECF14, Vol. 1,2002, pp. 209-216.

[23] Bartsch, M., Baufeld, B. and Fuller, E.: Elucidating Thermo-Mechanical Spallation of Thermal Barrier Coating-Systems using Controlled Indentation Flaws, Cocoa Beach, January 2003, in press.

[24] Pfaendtner, J.A. and McMahon Jr., C.J.: Acta Mater., 49, 2001, pp. 3369.

[25] Krupp, U., Kane, W.M., Liu, X., Dueber, O., Laird, C. and McMahon Jr., J.: Mater. Sci. Engng., 2003, in press.

[26] Staniek, G., Hillger, W. and Dalle Donne, C.: Ultrasonic Testing on Friction Stir Welded Aluminium Alloys, Welding and Cutting, 6, 2002, pp. 313-318.